Faulting and fault sealing in production simulation models: Brent Province, northern North Sea

S. J. Jolley[1], H. Dijk[1,2], J. H. Lamens[1,3], Q. J. Fisher[4], T. Manzocchi[5], H. Eikmans[1] and Y. Huang[1,2]

[1]*Shell UK Exploration & Production Ltd., 1 Altens Farm Road, Nigg, Aberdeen AB12 3FY, UK*
[2]*Shell International Exploration & Production, Volmerlaan 8, 2288-GD Rijswijk-ZH, Netherlands*
[3]*Badr Petroleum Company (Bapetco), 127 Abd Elaziz Fahmy Street, Heliopolis, Cairo, Egypt*
[4]*Rock Deformation Research Ltd, School of Earth Sciences, University of Leeds, Leeds LS2 9JT, UK*
[5]*Fault Analysis Group, School of Geological Sciences, University College Dublin, Belfield, Dublin 4, Ireland*

ABSTRACT: Faults can severely compartmentalize pressures and fluids in producing reservoirs, and it is therefore important to take these effects into account when modelling field production characteristics. The Brent Group fields, northern North Sea, contain a complex arrangement of fault juxtapositions of a well-layered sand-shale reservoir stratigraphy, and fault zones containing a variety of fluid flow-retarding fault rock products. It has been our experience that these fault juxtapositions impact the 'plumbing' of the faulted layering system in the reservoirs and the models that are built to mimic them – and are, in fact, a first-order sensitivity on compartmentalization of pressures and fluid flow during production simulation. It is important, therefore, to capture and validate the geological feasibility of fault-horizon geometries, from the seismic interpretation through to the static geocellular model, by model building in conjunction with the interpretation. It is then equally important to preserve this geometrical information during geocellular transfer to the simulation model, where it is critical input data used for calculation of fault zone properties and fault transmissibility multipliers, used to mimic the flow-retarding effects of faults. Application of these multipliers to geometrically weak models tends to produce ambiguous or otherwise potentially misleading simulation results. We have systematically modelled transmissibility multipliers from the upscaled cellular structure and property grids of geometrically robust models – with reference to data on clay content and permeability of fault rocks present within drill core from the particular reservoir under study, or from similar nearby reservoirs within the same stratigraphy. Where these transmissibility multipliers have been incorporated into the production simulation models, the resulting history matches are far better and quicker than had been achieved previously. The results are particularly enhanced where the fault rock data are drawn from rocks that have experienced a similar burial–strain history to the reservoir under study.

KEYWORDS: *fault model, fault geometry, fault seal, transmissibility multipliers, compartmentalization, Brent Group*

INTRODUCTION

In general terms, a static hydrocarbon column held across a fault is caused by aquifer and buoyancy pressure of fluids (applied against the capillary entry pressure of fault rocks and juxtaposed stratigraphies) reaching equilibrium across the fault over geological time (Fisher *et al.* 2001). This equilibrium is achieved at infinitesimally slow rates of flow, and often results in a common static hydrocarbon contact level across intra-reservoir faults. However, under production conditions, pressure gradients between wells induce flow rates within the reservoir sands that can be much faster than the rates achieved across these (much lower permeability) fault zones. Thus, pressures and the hydrocarbon saturations and contacts begin to separate into compartments across the faults, and between individual sand units flowing at different rates from each other across the faults (e.g. Childs *et al.* 2002). Fault seal analysis under production conditions therefore attempts to define the oil, gas and water rate of flow across the faults in order to quantify: (a) the 'effective' connected volumes that can be accessed at economic rates by any given well; and (b) the related rate interaction between a group of wells.

The tool used for these assessments is the flow simulation or 'dynamic' model, which is used in 'prediction mode' to guide business forecasts, field development, production management and well planning decisions (e.g. Dake 2001). The validity of the 'prediction mode' of a model is tested by comparing the match

1354-0793/07/$15.00 © 2007 EAGE/Geological Society of London

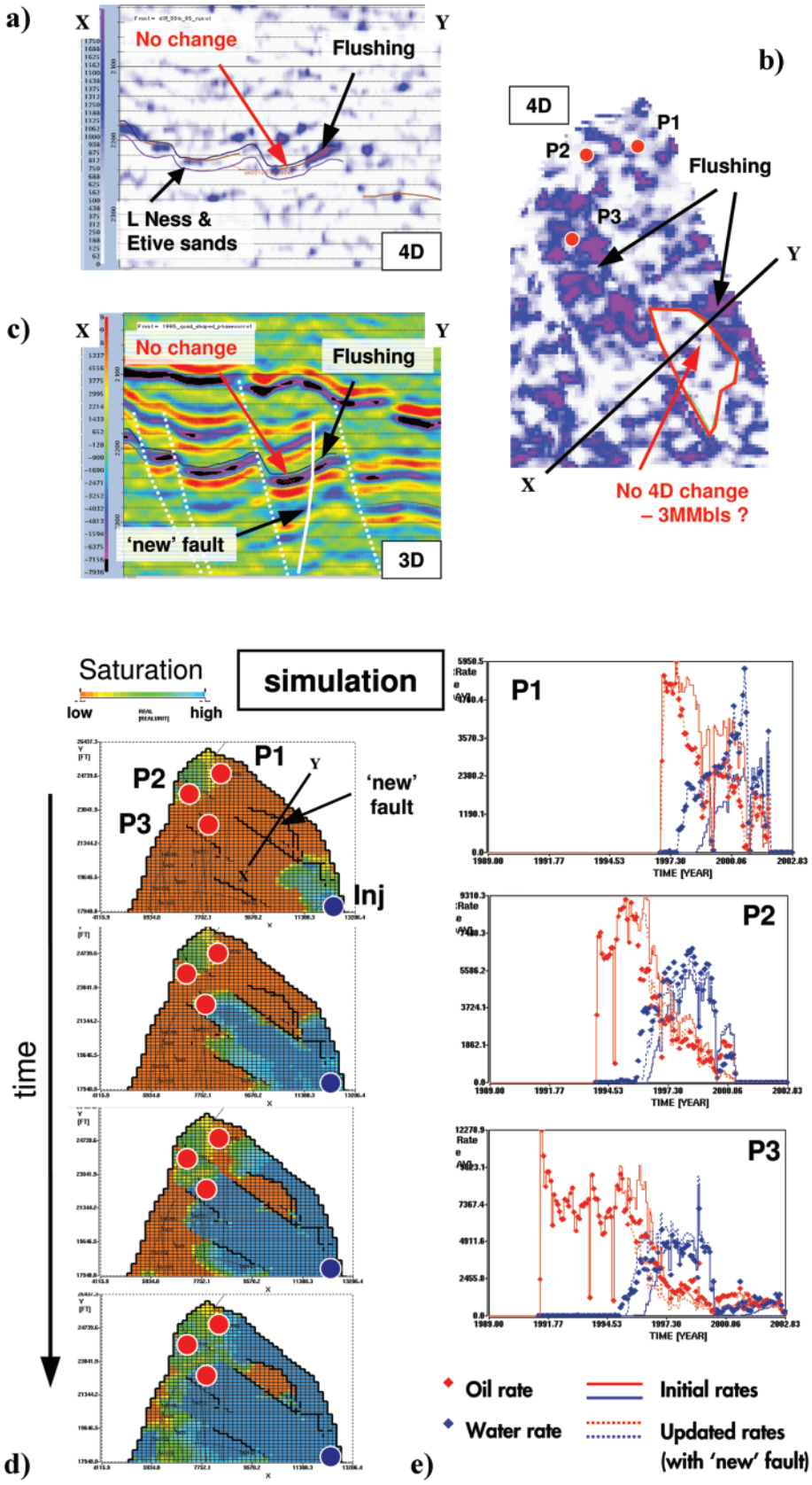

Fig. 1. Diagram showing the impact of an intra-reservoir fault on fluid flow. (**a**) and (**b**) show a potentially unswept compartment, identified in 4D seismic sections and maps (red polygon). (**c**) Re-examination of the 3D seismic data revealed a previously uninterpreted fault, which mapped out along the curved eastern edge of the 4D signal. This coincidence suggested that the fault retarded flow sufficiently to act as a sweep barrier in the reservoir. (**d**) The fault was incorporated into the simulation model for the field to examine its effect on fluid production in three crestal producers, being supported by a downflank water injector. Inclusion of the fault dramatically altered the sweep pattern. (**e**) The production simulation was improved greatly by inclusion of the fault – with the simulated oil and water rates in the three wells now matching the actual data.

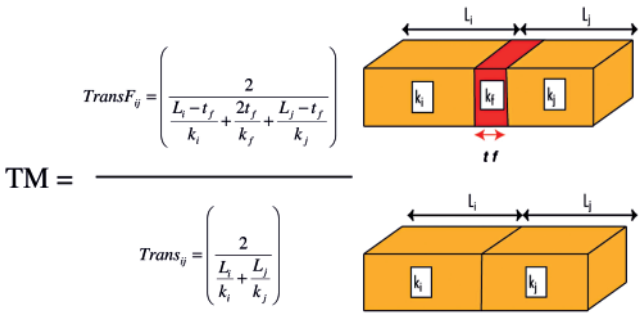

Fig. 2. Conceptual cartoon of fault transmissibility multiplier (TM) calculation between faulted cells of a simulation model. These calculations differ in detail between simulation software packages and this particular cartoon (modified from Manzocchi *et al.* 1999) ignores cell dip terms and assumes net-to-gross ratios and intersection areas of 1.0.

between actual historical production data and the simulated production history, increasingly in recent years in conjunction with use of 4D seismic data (e.g. Fig. 1; Staples *et al.* 2002, 2005; Lygren *et al.* 2003; Waggoner *et al.* 2003). The stratigraphic controls on field compartmentalization are addressed within generally accepted subsurface tools and workflows. However, it has been an industry-wide experience that surprisingly little time and technology is set aside to capture, quantify and integrate the effect of faults on reservoir connectivity and flow behaviour into a typical simulation model. Thus, whilst a 'model' history match can be achieved by incorporating unrealistic faults and fault properties, this may be an artificial compensation for other hidden inadequacies in the model (Fisher & Jolley 2007). Hence, the distribution of fluids connected across the faults in a field, as controlled by the juxtaposition arrangement and fluid flow properties of the faults, has remained one of the largest uncertainties in the subsurface assessment. This impacts prediction of a field's production efficacy, and the planning of drilling to optimize hydrocarbon sweep (e.g. Corrigan 1993; Lia *et al.* 1997).

The flow of fluids between adjacent cells in a simulation model is controlled by the cell–cell transmissibility (a function of the geometry and properties of the cells). However, the reduced permeability characteristics of an intervening fault should retard the flow across sand–sand juxtapositions. This effect is accounted for by correcting the cell–cell transmissibility with a fault transmissibility multiplier (a function of fault rock thickness, permeability and cell properties; Fig. 2). Traditionally, these flow-retarding effects of faults are addressed late in the workflow by the reservoir engineer, who imposes transmissibility multipliers on the faults, in some cases adding or removing faults from the model. However, this is essentially educated guesswork, which manually steers pressures and fluid flow within the model and frequently results in unrealistic 'special' treatment of some faults in the model. In geological terms, this treatment would imply that these faults were developed under radically different physical-chemical conditions to their neighbours. Clearly, this approach does not mimic the complex, three-dimensionality of faulted sand juxtapositions or the systematic porosity–permeability variations that characterize natural faults. Given that flow within a simulation model is a function of its input geocellular grids and that it is sensitive to the various *ad hoc* parameter amendments applied by the engineer to achieve a history match, no simulation is a unique model solution for the field. Thus, the more of these amendments there are in a model, the less likely it becomes that the simulated flow approximates to reality (despite the production history match). Consequently, the forecast mode of the model becomes increasingly unreliable.

This paper describes how this uncertainty can be reduced greatly, through the constraints that are imposed on the model by inclusion of geologically realistic faults, integrated with systematically calculated fault zone properties (e.g. reduced porosity and permeability). The first step in ensuring that this takes place is the provision of a geometrically 'realistic' horizon-fault interpretation of the seismic data as a basis to build a structurally valid geological static model. Following this, the accurate import and preservation of the geocellular information from the static model into the simulation model ensures validity of fault architectures and juxtapositions. This is, in fact, a basic prior requirement for effective calculation and integration of fault transmissibility multipliers in the simulator – since most fault seal-related algorithms are based on fault displacement and the properties of the near-fault stratigraphy (see below). We then integrate these geologically valid fault geometries with geologically reasoned fault transmissibilities in the simulator – as calculated from the upscaled geocellular grid – to produce unique transmissibility multipliers for each across-fault cell–cell connection in the model (*sensu* Manzocchi *et al.* 1999, 2002).

In this paper, we describe the application of an approach that has been found to be successful under the 'battle conditions' of live asset projects, and which is rooted in the pragmatic experience of the authors. Several case examples are used to illustrate the effectiveness of these methods in capturing the fluid flow properties of faults and faulted reservoir connectivity. It is shown that this is capable of generating a step-change improvement in history match without requiring iterative *ad hoc* edits to model parameters – thus improving confidence in the model's forecast mode. The examples come from mature Brent Group fields in the northern North Sea, where the method can be tested unambiguously with the production history match in several fields that each have 20–30 years' production data from 2–300 wells (Fig. 3). Finally, the role and validity of the single-phase transmissibility multiplier method described here is discussed within the wider context of more recent developments in faulted multi-phase flow concepts and methodologies.

GEOLOGICAL CONTEXT OF THE BRENT GROUP FIELDS, NORTHERN NORTH SEA

This section of the paper outlines the reservoir geology, with emphasis on the geometry and timing of movement on the fault arrays. This information is important as input to understanding the nature of the basic fault juxtaposition of sand flow units, and the prevailing physical-chemical conditions that control the development of various types of flow-retarding fault rocks.

Stratigraphy

The Middle Jurassic Brent Group stratigraphy is subdivided into five major lithostratigraphic units (the **B**room, **R**annoch, **E**tive, **N**ess and **T**arbert formations, Deegan & Scull 1977), which were deposited in a variety of shallow-marine to coastal-plain environments (Hampson *et al.* 2004, and references therein). The sequence 'motif' can be subdivided into three parts: a lower panel composed of a variety of bioturbated to clean fine–medium-grained laterally persistent sands, silts and shales, overlain by more massive sands; a mid section composed of shales; and an upper package composed of a depositionally complex suite of laterally persistent shales, silts, sands and locally developed coals, which become coarser and more bioturbated towards the top (Fig. 3). The detailed depositional content of the sequence and erosive quality of intra-Brent

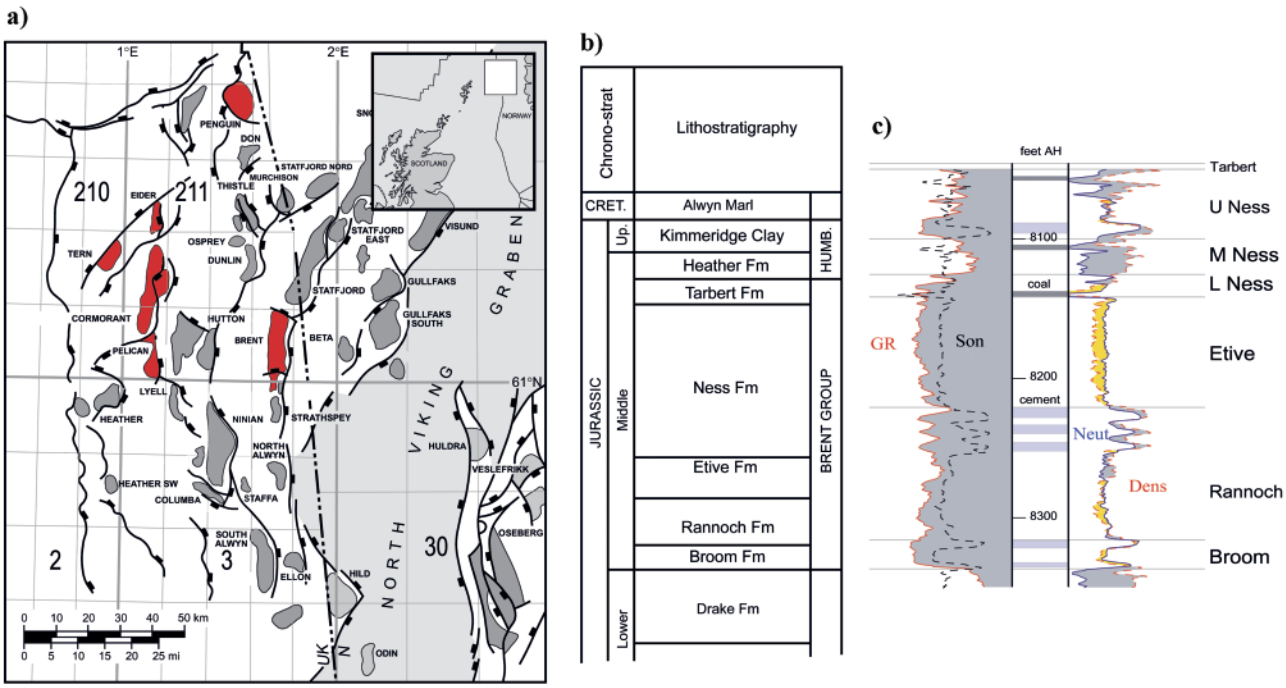

Fig. 3. (**a**) Location map and fields in the Brent Province northern North Sea; fields involved in this study are indicated in red (modified from Underhill *et al.* 1997). (**b**) Stratigraphy, Brent Group. (**c**) A typical Brent Group well, showing gamma ray (GR), sonic (Son), Neutron (Neut) and density (Dens) geophysical log responses. This combination of logs can be used to differentiate the distribution of clay content within the sequence from locally developed coals and 'dogger' cement zones.

unconformities at any given point vary with respect to the position of the palaeo-shoreline, although the overall depositional thickness of the sequence remains fairly constant. The general exception to this is the uppermost part of the Ness and Tarbert formations, which have been shown locally to contain growth against normal faults, which were beginning to develop at the outset of the widespread late Jurassic–early Cretaceous rifting in the North Sea (e.g. Ziegler 1990; Thomson & Underhill 1993; McLeod *et al.* 2000, 2002).

Structure

The Brent Province oil fields lie within the footwalls of major half-graben of this age, which form regional terraces along the margins of the Viking graben system. The Brent Group thickens very gradually to the east regionally and across individual fields, and there are locally developed fault-growth sequences in the Tarbert Formation, in particular. However, the upper part of the Brent is often thinned by erosion and/or non-deposition towards the crestal areas of the fields, beneath the Heather shales, where footwall uplift on the margins of the local graben would have been most active, perhaps causing subaerial exposure at the time. The late Jurassic–early Cretaceous faults overprint and rework an earlier, equally significant rift system that had developed during the Triassic and even older Variscan structures and Caledonian-age lineaments and fabrics within the basement (e.g. Yielding *et al.* 1992; Roberts *et al.* 1995; Færseth 1996). The Jurassic–Cretaceous fault arrays formed by a combination of new segment propagation and selective reactivation of pre-existing faults. Thus, some old normal faults became reactivated and incorporated within the plane of the main trend graben, whilst others became re-utilized as displacement-relaying cross-faults and strike-slip faults, to form a rhomboidal fault pattern across the region. The trend, spacing and throw variation of fault arrays are also seen to be partitioned by a combination of hard- and soft-linkage across Triassic structures and older basement lineaments. This reworking of faults to perform new kinematic functions is a common structural process (e.g. Peacock & Shepherd 1997; Jolley *et al.* 2007), as is the selective reactivation of basement fabrics and fault arrays to form rhomboidal fault patterns during oblique rifting (e.g. Khalil & McClay 2001; Younes & McClay 2002; Morley *et al.* 2004; Bellahsen & Daniela 2005).

The late Jurassic–early Cretaceous fault arrays in the region can be subdivided into two kinematically and geometrically distinct groups: a thick-skinned (basement-attached) fault system of major graben and smaller cross-faults, as described above; and thin-skinned fault arrays that form contemporary slope instability (landslide) complexes (Welbon *et al.* 2007), parochially referred to as 'slumps'. For example, the famous Brent Field dips to the west in the footwall to a major easterly dipping normal fault. It is confined at its northern and southern ends by smaller, broadly E–W to WNW–ESE-trending normal cross-faults, which appear to reactivate older faults in the underlying basement. The immediate footwall to the field's eastern boundary fault, is disaggregated by an easterly transporting slump complex (Fig. 4). The economic value of understanding the relative volumes and fluid connectivity between these groups of structures is shown by total ultimate production, estimated in 2003 at approximately 2000 MMBL oil and 6000 BCF gas, with approximately 10% coming from the slumps (Taylor *et al.* 2003). The slumps are internally complex, comprising linked arrays of N–S-trending normal faults which detach into shale packages within and beneath the Brent Group reservoir sequence. These structures subdivide the reservoir into an array of blocks (ranging from 50 × 500 m to 200 × 1700 m in map area), but lose coherence and degrade into a rubble or slurry zone downslope. These slumps are underlain by a later, second tier of slumping which disaggregates the Statfjord reservoir zone. This lower slump complex is composed of arrays of larger, listric faults and rotated blocks which

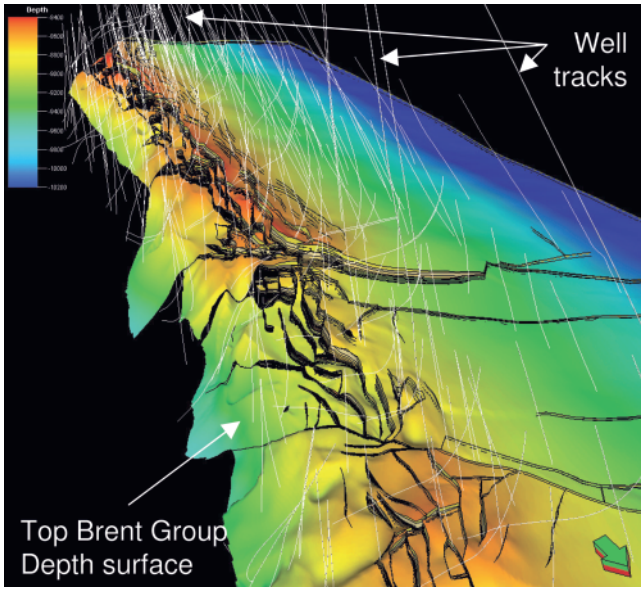

Fig. 4. General view of Brent Field structure looking south. Note steep basement-attached broadly E–W-trending faults that dissect the field into sub-blocks; and broadly N–S-trending arrays of thin-skinned slump faults at the crest of the field. The slumps are partitioned by the steeper faults, which have been locally reworked to form lateral ramps in the slump complex. Also, note dense well coverage (white lines) drilled from four platforms, as discussed in the text.

are less confined or influenced by stratigraphic detatchments – appearing instead to 'flatten' towards the foot of the contemporary free surface, exposed by the downward movement of the hanging wall to the field-bounding normal fault. They, therefore, take the geometrical form of large-scale 'rotational failures', more commonly described as instability hazards within civil engineering and open-pit mining operations. This pattern of stacked slump complexes is also seen in the Statfjord Field, which lies along-strike immediately to the north (Hesthammer & Fossen 1999; Welbon *et al.* 2007) and is repeated in general terms within most of the fields in the region (e.g. Underhill *et al.* 1997; Berger & Roberts 1999). The thin-skinned slump arrays are linked spatially and kinematically to the thick-skinned faulting, via a combination of hard- and soft-linked fault geometries. Thus, the geometry, spacing and displacement variations within the arrays of faults in the slump complexes on some fields are clearly seen to be partitioned across the line of thick-skinned cross-faults and basement lineaments (Fig. 5). There are variations on this general theme, ranging from some fields having very narrow, steep extensional imbricate arrays linked to the main graben fault, grading into broad detached imbricate arrays and slurry zones, and to major footwall rotational failure zones spanning the entire width of a field (e.g. Gullfaks, Welbon *et al.* 2007; North Cormorant).

The Heather and Kimmeridge shales onlap these Brent/Statfjord slump complexes. However, a further panel of slumping is often developed within the Upper Heather and Kimmeridge shales, in particular. In the Pelican and Cormorant fields, these younger slump structures appear to detach somewhere within the middle of the Heather shales, whereas the Lower Heather is displaced by the thick-skinned faults, which rapidly tip-out at this level (Fig. 6). The Heather–Kimmeridge slump structures transport eastwards into the hanging wall of the field-bounding faults, occasionally truncating the crestal area, and also form broad arrays of faults which transport westwards and down local palaeo-slope above the field flanks,

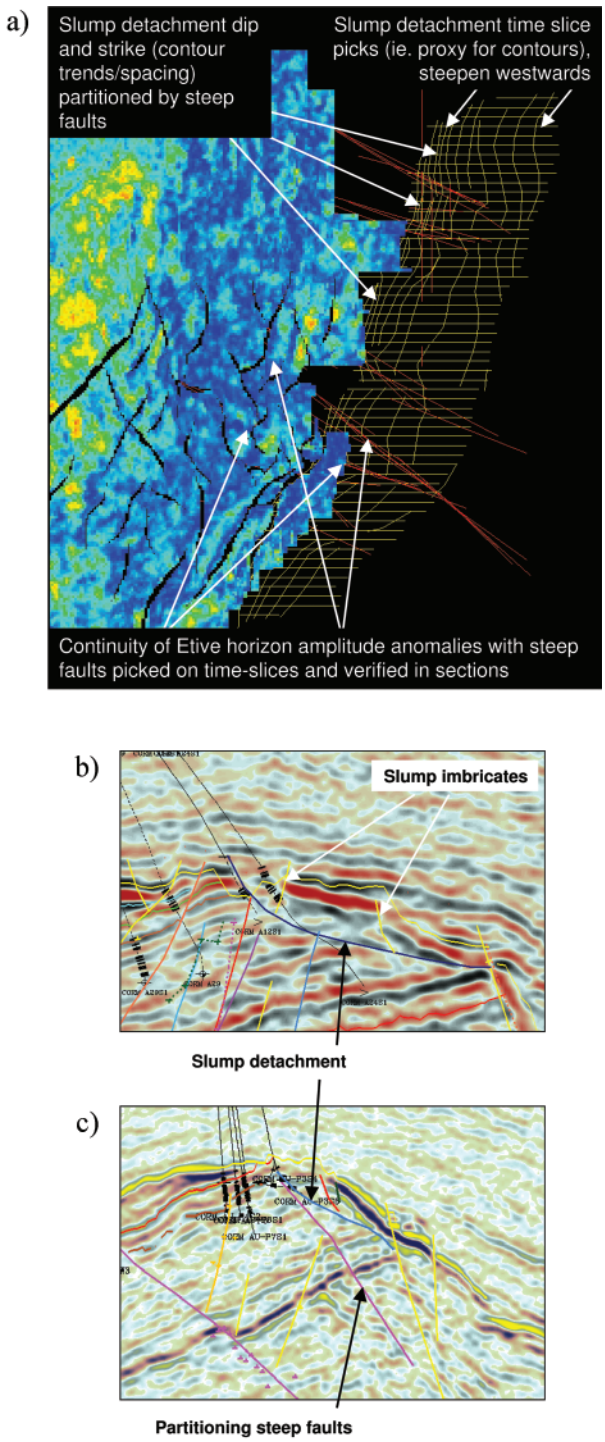

Fig. 5. Diagram showing kinematic linkage between steep 'thick-skinned' faults and 'thin-skinned' slump complexes. (**a**) Map showing steep faults (red lines picked on time-slices) and slump detachment (yellow lines picked on W–E sections and time-slices) and an amplitude extraction from the Etive reflection, South Cormorant. Note that the steep faults are contiguous with linear amplitude anomalies in the main body of the field and that the slump detachment changes dip and dip direction across the steep structures (the yellow time-slice picks are equivalent to contours). This indicates that the earlier steep Triassic(?) faults were part-reactivated and incorporated as lateral ramps within the slump complex. (**b**), (**c**) W–E seismic sections through the slumps, showing the linkage between the slumps and local reworking of the steeper faults.

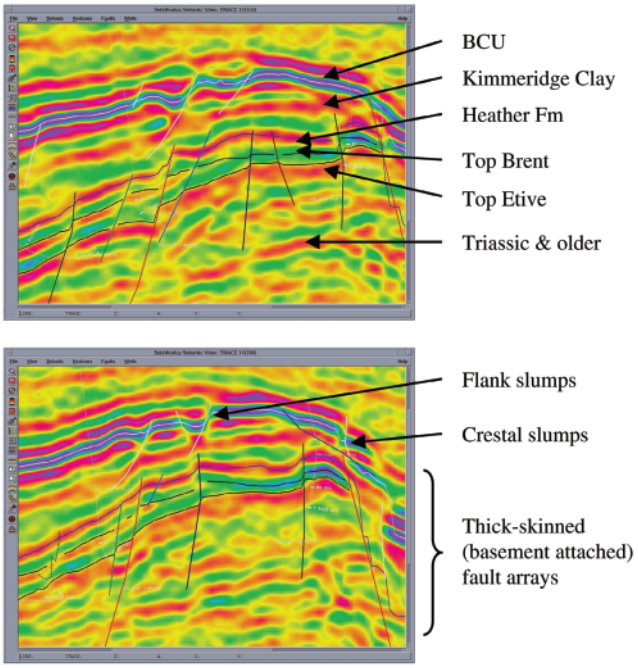

Fig. 6. Seismic sections looking north, showing the general structure of the Pelican Field. Steep thick-skinned faults in the main body of the field; thin-skinned slumps at the crest of the field; and thin-skinned slumps within the Upper Heather and Kimmeridge at the flank of the field. Also, note eastward thinning of the upper Brent sequence towards the crest of the field. BCU, Base Cretaceous Unconformity.

with offset soft-linkage to underlying thick-skinned fault scarps (Fig. 6). These particular slumps enable the Base Cretaceous Unconformity to retain a relatively constant, shallow dip across the area of a field, even though the Brent Group dip and depth may vary along-strike. This is interpreted to indicate that they formed in response to the process of Kimmeridge shales, in particular, slumping and otherwise deforming internally to retain a critical angle of slope stability, driven by fault-controlled movement of the substrate (block tilting, footwall rebound and uplift) during the end Jurassic–early Cretaceous rifting.

Summary

- The Brent Group contains a well-defined essentially sand–shale stratigraphic layering system. In broad terms, this divides the fields into an upper and lower reservoir series (separated by the Mid-Ness-Shale), with laterally continuous shale beds further subdividing the reservoirs into more discrete flow units.
- The fields contain a complex arrangement of fault juxtapositions arising from a combination of linked steeply- and shallowly-dipping fault arrays. Thus, sandbody connectivity and/or compartmentalization across the faults is three-dimensionally complex.
- The faults affecting the Brent Group were active during deposition of some of the later reservoir units and in the immediate period afterwards, when Heather and Kimmeridge shales were being deposited. Thus, the faults were active when the Brent Group reservoirs were at near-surface to shallow burial depths, and were then buried passively with host stratigraphy to reach their present-day depth positions.

WHY DO FAULTS IMPACT RESERVOIR PRODUCTION?

Fluid flow and pressure in an oil field is compartmentalized by a combination of stratigraphic and structural architectures. Current subsurface tools and workflows routinely include detailed characterization of the depositional architecture of a given reservoir, its lithofacies and associated mineralogical and porosity–permeability property variations. These variations are captured at geological scale within the 'static' geocellular reservoir model, and upscaled to become the flow simulation model for the field. Thus, in siliciclastic reservoirs, stratigraphic barriers and baffles to vertical flow are captured explicitly by the relatively shale-rich layers in the model and lateral barriers and baffles by the intra-layer architectures, such as channels and pinchouts. However, assessment and account of lateral flow barriers and baffles at faults is often incomplete. Frequently, it is assumed that this is entirely due to fault juxtaposition of reservoir sands with non-reservoir stratigraphy. Even if time and effort are given to accurate modelling of valid fault geometries, the true effect of juxtapositions on flow connectivity is complicated by the fact that there are no 'clean' juxtapositions in nature. In detail, a fault plane interpreted from seismic data is not a discrete surface – but rather a 'fault zone' within which the well-ordered host stratigraphy is smeared, disarranged and re-aggregated (e.g. Fig. 7; Childs *et al.* 1997; Foxford *et al.* 1998; Aydin & Eyal 2002; Rykkelid & Fossen 2002; van der Zee *et al.* 2003; Davatzes & Aydin 2005; Kristensen 2005). Fault zones are generally composed of a hierarchical assemblage of meso-scale faults and halos of smaller-scale faults and fractures, which host a variety of fault-rock types and mineral fills (e.g. Fig. 7; Caine *et al.* 1996; Fisher & Knipe 1998; Beach *et al.* 1999; Odling *et al.* 2004; Berg & Skar 2005; Shipton *et al.* 2005). The disruption to flow caused by the complex juxtaposition of flow baffles and conduits across and within the faults is, therefore, compounded by the retarding effects of the fault rocks, and related tortuosities imposed on the flow pattern by the fault zone architecture.

The exact suite of fault rocks that form within the fault zone varies systematically with the prevailing physical-chemical micro-scale deformation mechanisms. In turn, these are controlled by factors such as the clay content and grain size of the protolith as well as the pre-, syn- and post-deformation stress and temperature history (e.g. Fisher & Knipe 1998, 2001; Fisher *et al.* 2000; Sperrevik *et al.* 2002). For example, where faulting occurs in high net-to-gross sands near to the surface, the dominant micro-scale deformation mechanism is particulate flow. Individual sand grains pop out of their packing order and revert back to a similar packing order once the fault has stopped moving, without significant grain fracturing, to form fault rocks called 'disaggregation' zones. The resultant permeability is, therefore, little different to that in the undeformed host sands (Fig. 8). However, if the same sands were deformed at greater burial depth (>1 km), there would be sufficient stress for fracturing and crushing of individual grains to occur – resulting in overall grain-size reduction to form 'cataclasites' with permanent porosity–permeability collapse (Fig. 8). Microstructural observation of fault rocks obtained from Brent Group drill core indicates that faulting deformation generally occurred with negligible grain fracturing (Fisher & Knipe 2001). This is consistent with seismic and drilling data (described above), which indicate that faulting in the Brent fields took place under shallow burial conditions.

Impure sands (15–40% clay) deform during shallow burial to produce 'phyllosilicate-framework' fault rocks. Deformation-induced influx of clay particles from the surrounding matrix

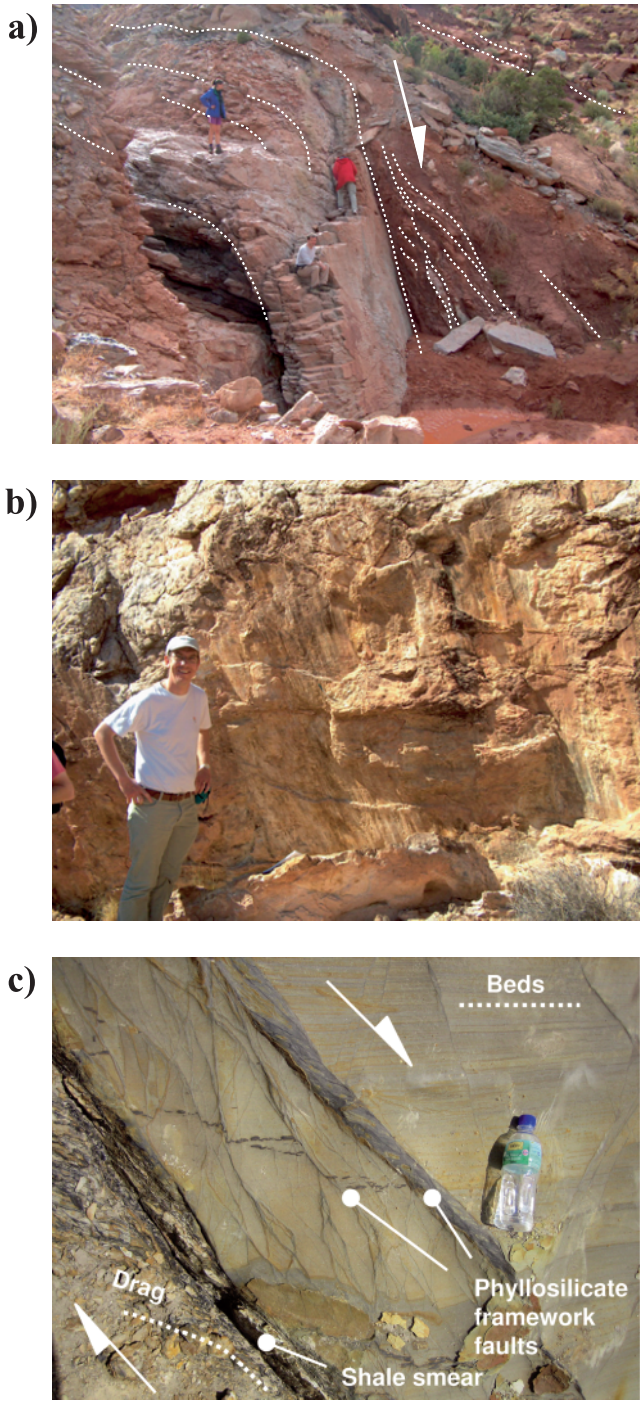

Fig. 7. Field photographs of fault zones: (**a**) meso-scale sand–shale smears (Moab Fault zone, Utah, USA); (**b**) swarms of cataclastic slip planes containing strong slickenline lineations (Moab fault zone, Utah, USA); (**c**) clay smears and damage zone of phyllosilicate framework faults and shear fractures (Amin Farm, Miri, Sarawak).

and mixing of these particles with the framework grains in the fault, results in a rapid decrease in porosity and permeability (Fisher & Knipe 1998, 2001). Faulting of discrete shale beds often results in the formation of clay smears in the faults (Fig. 7, Fig. 8), which often have permeabilities under 0.1 μD, below that of the source shale beds (Fisher & Knipe 2001; Eichhubl *et al.* 2005). The moderate to severe porosity–permeability reduction that occurs due to the deformation of impure sands and clay-rich layers may continue during burial, long after faulting has taken place, since the presence of clay minerals enhances grain-contact quartz dissolution in the fault zone (Fig. 8; Sverdrup & Bjørlykke 1992; Fisher & Knipe 1998, 2001; Sperrevik *et al.* 2002).

Thus, in general terms, the permeability of fault rocks is related to their clay content and the syn-kinematic and post-deformation stress–temperature history. This can have a profound effect on the variability of sealing/baffling behaviour of faults within a reservoir under production conditions (e.g. Hesthammer *et al.* 2002). The majority of faults in the Brent Group reservoirs experienced a single movement phase, causing syn-kinematic permeability collapse at relatively shallow (0–500 m) depths; and then further permeability collapse of the clay-rich fault rocks, in particular, during the subsequent relatively simple passive burial. Thus the present-day depth of a specimen taken from drill core, can be considered as a crude proxy for this later stress–temperature-driven permeability collapse. This is illustrated by the fault rock data measured in drill cores from Brent Group reservoirs shown in Figure 9. The data show basic clustering of the fault rock permeability (reduction) as a function of fault rock type, clay content and burial depth. As a general rule, cataclasites are not a common fault rock type in Brent Group faults (though included in Fig. 9) and tend to be associated with those particular faults that have experienced later reactivation under greater burial depths and temperatures.

In summary, it is therefore possible to quantify broadly the variation of flow-retarding effects of the faults in the reservoirs discussed in this paper, where the distribution of clay can be determined within the model-scale fault planes. This modelled clay content can be compared with measured data on fault rock clay content and permeability, with some refinement possible by filtering of the data based on syn- and post-kinematic burial history (see below).

INTERPRETING AND PRESERVING VALID FAULT GEOMETRIES

As mentioned above, the primary structural influence on flow in the reservoir is the geometrical arrangement of sandy juxtapositions across the faults. Therefore, structural assurance of a simulation begins with capturing a valid fault-horizon interpretation from the seismic data, and then preserving this geometry through the static geocellular model and into the simulation model. Since seismic interpretation files form the skeletal frame for a structure model build, it is critical to: (1) ensure that these data form a geometrically valid entity in their own right; and (2) then avoid discrepancies arising between these geometries interpreted in the seismic data, and the static and simulation model builds (cf. Fig. 10).

Structure-seismic interpretation, framework and static modelling

Seismic reflection energy is disrupted by faults to produce a number of diagnostic signatures, which – depending upon the geology, the type of data in use and the scale and geometry of a fault – are present in various combinations (e.g. two-way-time offsets, changes in reflection character and dip, amplitude dimming, diffractions, fault-plane reflections, coherency edges). Faults picked from a combination of these diagnostic criteria can be subdivided loosely into those that are large enough to offset the two-way-time arrivals of reflections (enabling them to be identified on traditional section and time-slice data displays) and those with smaller throws close to the detection limits of the seismic survey (which can be imaged only by data 'attribute' variations) (cf. Fig. 11). One theoretical rule-of-thumb suggests

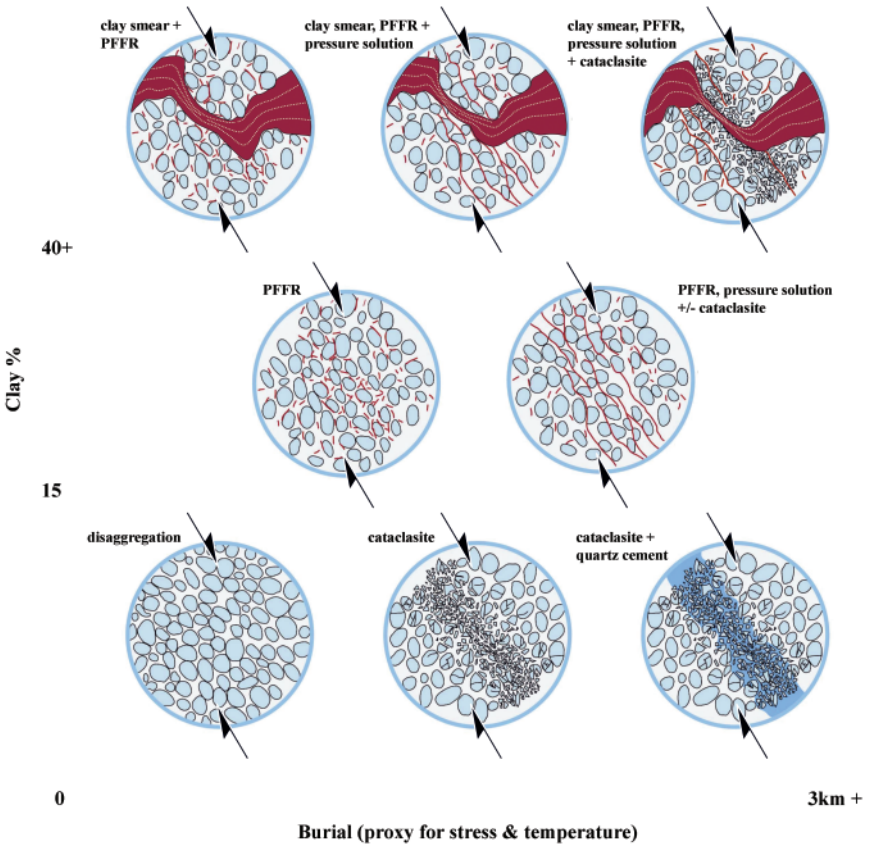

Fig. 8. Schematic cartoons of micro-structural processes within fault rocks, leading to permanent collapse of the host rock porosity–permeability structure, as a function of host clay content and burial depth. PFFR, phyllosilicate framework fault rock.

that the smallest fault throws that can be imaged by seismic amplitudes are equivalent to 1/4 of the dominant seismic wavelength (see Townsend *et al.* 1998, for discussion). However, direct comparison of seismic data with underground structural mapping in deep mine workings indicates that seismic throw resolution is often closer to 1/8 of the dominant wavelength of the data (e.g. Jolley *et al.* 2007; Fig. 11). Most interpretation and modelling exercises import the larger structures to the static model, supplemented by the smaller fault populations as appropriate.

In almost all cases of manual or automated interpretation, the horizon picks will not extend exactly to the local fault

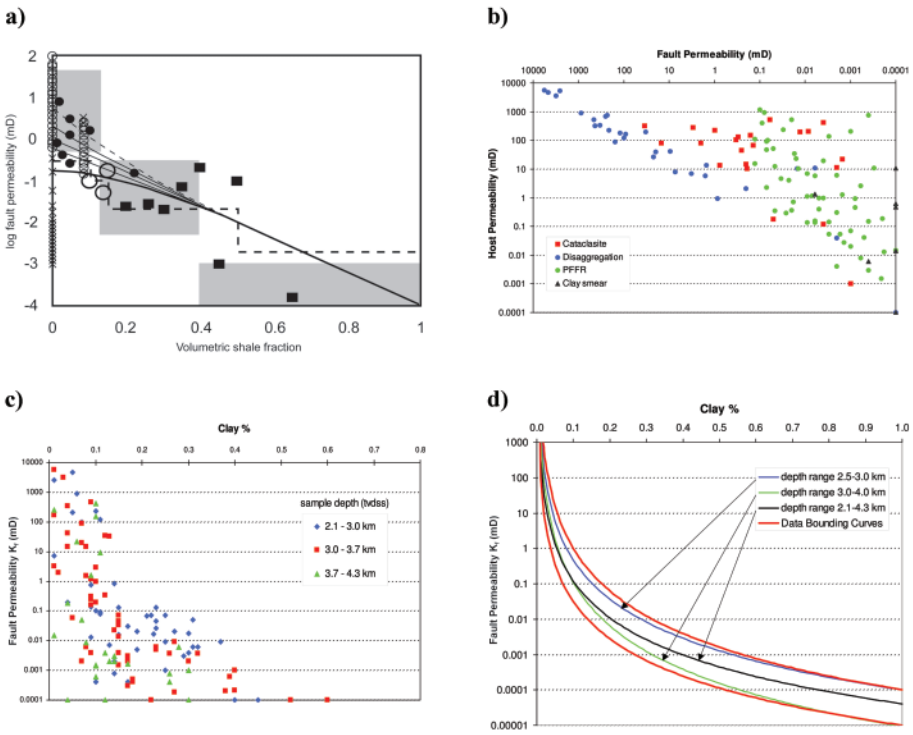

Fig. 9. Fault rock permeability data: (**a**) an example of an amalgamated dataset (after Manzocchi *et al.* 1999); (**b–d**) data measured from drill cores in Brent Group reservoirs within the study region (derived from Fisher & Knipe 2001, together with extra data gathered during this study). (**b**) Permeability (reduction) of different fault rock types compared to undeformed host rock permeability. Disaggregation faults show negligible permeability change, whereas clay smears show the most extreme reduction. Cataclasites and phyllosilicate framework faults show greatest scatter. (**c**) Fault permeability as a function of host clay content. Despite natural scatter, the data show some trend clustering as a function of burial depth range of the samples. (**d**) Brent Group fault permeability as a function of clay content and (burial) depth of sampled cores. The red curves represent the upper and lower bounds of the range of relations that can be derived from these data, whilst the black curve represents the whole dataset, and the green and blue curves are derived from sub-sets of the sample depth range equivalent to particular study reservoirs (see text for details).

segment. In practice, the dip of reflectors and, therefore, any horizons based on them, become unstable near to faults in the seismic data, such that the horizon terminations are often ragged and the fault segments they are meant to terminate against are also often jittery in the interpretation. Whilst de-spiking of horizon data at this stage helps – smoothing of the data destroys valuable geometrical information (e.g. fault throws needed to build the static model) and amplifies gridding instabilities within the static modelling process. To ensure geometrical validity and consistency, it is recommended that a structure framework (fault-horizon) model is built in conjunction with the seismic interpretation, using a framework building tool specifically designed to model and analyse structural geometries (e.g. Needham *et al.* 1996; Rutten & Verschuren 2003). This produces fault surfaces and horizon surfaces that form a structurally valid, interlocking horizon-fault framework. Within this framework, the line of intersection between a horizon and a fault plane that displaces it, is separated into a hanging-wall cut-off and a footwall cut-off. These cut-offs taper towards closure at the geological tip line of the fault, where there is no displacement (Fig. 11). It follows that the fault throw in the model should not be less than the throw resolution of the seismic data adjacent to fault picks imported from the seismic interpretation. The zero-throw geological tips (and topologically valid fault–fault and horizon–fault intersections) are constructed within the structure framework model by various projection methods inherent within the framework-building software, guided by analogue structural data.

Within a seismic interpretation and the related framework model, the horizon cut-off lines are defined by 'fault polygons' on the fault surfaces. These polygons can be used as input data for static modelling, since they lie within the plane of the fault and, therefore, cleanly define the dip and geometry of the fault planes where they pass through the reservoir. The polygons, together with a closely-spaced x–y–z point-set up-sampled from the horizon surfaces in the framework model, effectively define a consistent structural geometry in their own right (Fig. 12). Since the horizon point-set data fit seamlessly into all corners of the fault model, use of this type of data constrains the gridding instabilities in most modelling situations. Thus, the structure framework model is re-generated reliably and quickly as the geometrical envelope within the static model, thereby ensuring geometrical validity and equivalence between the seismic interpretation and the static model (Fig. 12).

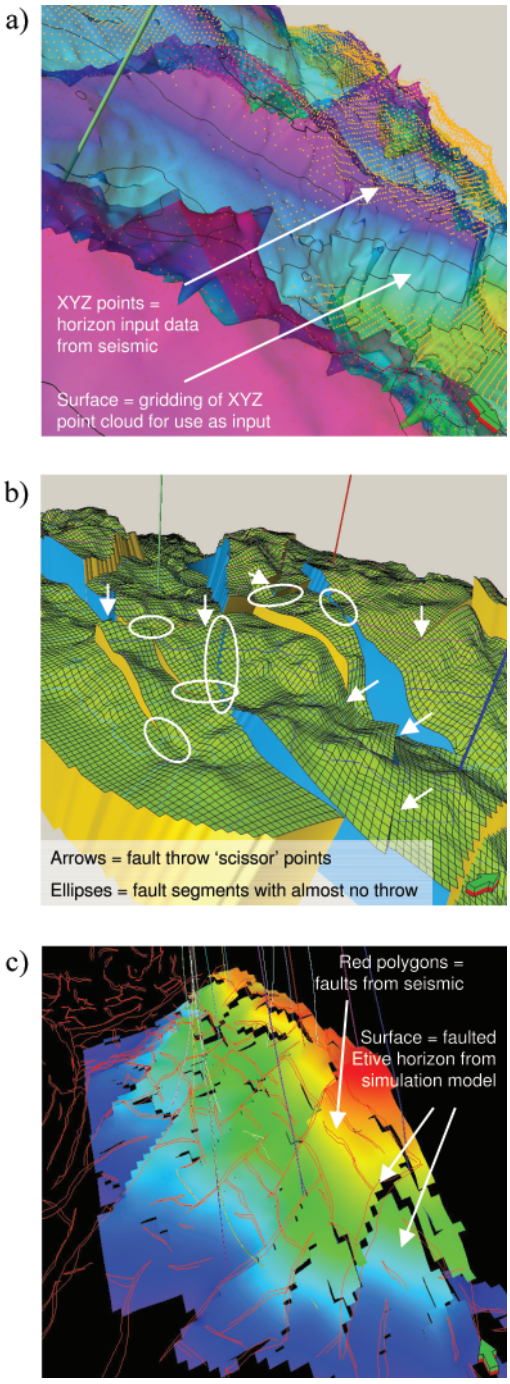

Fig. 10. Examples of bad practice (**a**) The x–y–z horizon data cloud imported to the static model from the seismic interpretation is excessively rugose, with common loop skips and spikes, and is geometrically invalid (inconsistent throws and interpolations across faults). A surface has been made from the data cloud and this surface was then used as the 'input data' for the horizon modelling. (**b**) This has resulted in a fault-horizon model, which is geometrically invalid. For example, fault throws diminish to near-zero in many places (ringed by dotted ellipses) and most of the faults hinge/scissor throw direction along-strike (arrowed). For clarity, only those errors in the foreground are highlighted. To generate the variation of movement vectors required on all the faults in this model, the fault blocks would have to undergo significant, unfeasibly complex independent motion and internal shape-change to stretch, compress and twist into position without opening holes or overlapping at the corners across the fault planes. Furthermore, faults are not imaged by seismic reflection data where throws are less than equivalent to 1/8 to 1/4 dominant seismic wavelength (see Fig. 11). Thus, the faults in the model should have coherent, consistent throw senses and should not be less than *c.* 10 m where they coincide with seismic fault picks. (**c**) An example of a disconnection between the fault-horizon geometries within the production simulation model and the original structure-seismic interpretation. In this case the top Etive (surface with zig-zag tears), has been exported from the simulation model into the static model for visualization in the same 3D space as the seismic interpretation of faults at the equivalent level (red fault polygons). There are radical differences between the two sets of faults and fault throws. The static model faults – not shown here for clarity – have an intermediate geometry.

Preservation of geometries in transfer from static model to dynamic model

Accurate preservation of this geometrical equivalence during transfer from the static model to the dynamic simulation model is critical to maintain the appropriate connectivity of reservoir sands across the faults. However, the transfer often requires some degree of 'upscaling' to simplify the cellular dimensions and properties in the model in order to reduce the complexity

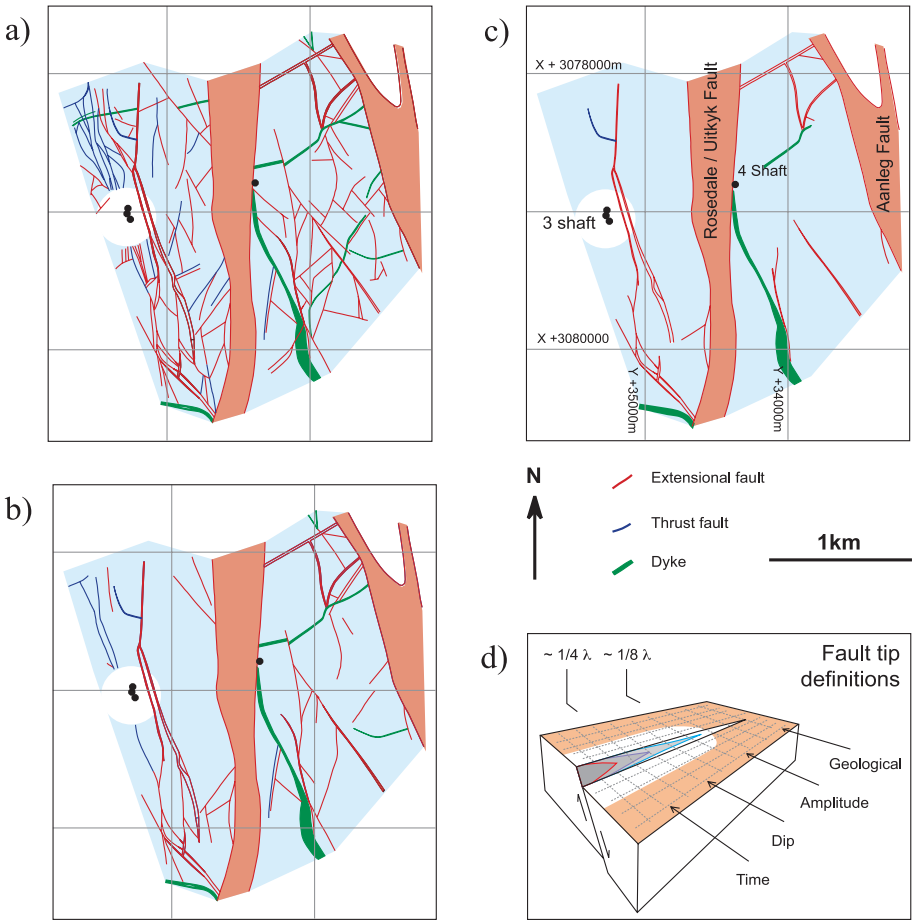

Fig. 11. Fault maps from stoped-out areas of a deep gold mine in South Africa, showing the connectivity of fault patterns as a function of geological and seismic throw resolution in locally acquired 3D vibroseis surveys. (**a**) All geologically mapped faults down to practical underground working resolution, equivalent to 1 m stope height. (**b**) Faults with 10 m or more throw. (**c**) Faults with 25 m or more throw. (**d**) Differences in fault throw resolution of various seismic data attributes, expressed as a proportion of dominant seismic wavelength, as measured directly by underground structure mapping in deep mines within seismic cubes. Acoustic impedance, frequency content etc. alter the exact relative throw resolution of the different attributes, although, in general, two-way-time offsets of reflectors image faults down to *c.* 1/4 of the wavelength and dip and amplitude attributes down to *c.* 1/8 of the wavelength (after Jolley *et al.* 2007).

of pressure and saturation-flow calculations and, therefore, the overall run-time of a production simulation. Thus, there is a tension between the two key aims of upscaling: to satisfy the practical needs of the simulation by reducing the geological complexity of a model to its salient characteristics; and to ensure that these key elements of the geology are preserved during the upscale. This is, therefore, a process that requires sensitive handling in order to avoid damage to the plumbing/flow characteristics of the model. Lateral (x–y) upscaling to increase cell size and/or discretize the cells to form orthogonal grids can cause severe damage to the fault geometries and reservoir juxtapositions across them, since it causes widespread changes to the fault positions, lengths, linkages, throws and surface areas. This is a particular problem where branching fault arrays may become disconnected and some faults 'loop' around the upscaled model. In severe cases, the reservoir engineer may have omitted 'problem' faults from the final model altogether. The impact of accepting incomplete fault arrays in a simulation model is illustrated in Figure 1.

However, if the static model is built to honour the framework fault geometries – at a cell size that is at or close to the size to be used in the simulation model – the model geometry can be transferred to the simulator with little or no lateral upscale. This method preserves the geometry of the static geocellular fault model. The benefits of preserving the geologically valid fault geometries from seismic interpretation to static model to simulation model in this way, are illustrated by the example shown in Figure 13. This compares the attempts to history match two simulation models that were based on the same basic static model. The only difference between the simulation models is that one was laterally upscaled (damaging the geometry), whereas the other was transferred as a 'realistic' model without geometrical upscale. The static model is shown with the top layers removed to reveal the relative position of the faults in the static model with respect to: the seismic structure framework faults that were used as input data (red polygons); and the position of the simulation model fault planes (black 'blades').

These models were run 'traditionally', starting with simple global fault transmissibility multipliers, which allowed an unambiguous test of the effects of fault array and juxtaposition geometry on the flow simulation. Simulation model 1 (Fig. 13a) was upscaled laterally from the static model by a factor of four (i.e. 25 × 25 m to 100 × 100 m) and discretized, causing widespread damage to the fault geometries. The reservoir engineer had a 'traditional' iterative struggle with the model variables, which evolved into a long list of significant *ad hoc* edits, including a five-fold multiplier on stratigraphic permeability, adding extra fault lengths, deleting fault segments and applying unique local fault transmissibility multipliers. After more than 225 runs, the engineer was unable to bring the model close to achieving a history match and the excessive level of *ad hoc* edits had undermined confidence in the model to measure or forecast production realistically. Simulation model 2 (Fig. 13b) was derived from a static model built at the required 100 × 100 m cell size to honour the geometrically valid structure framework model, and was transferred to the simulator without any upscaling. This model flowed immediately, with no permeability multipliers on any stratigraphic layers, and only required a few iterations with a few minor *ad hoc* edits to come near to a history match in about 70 runs, including sensitivity analyses, before the exercise was stopped.

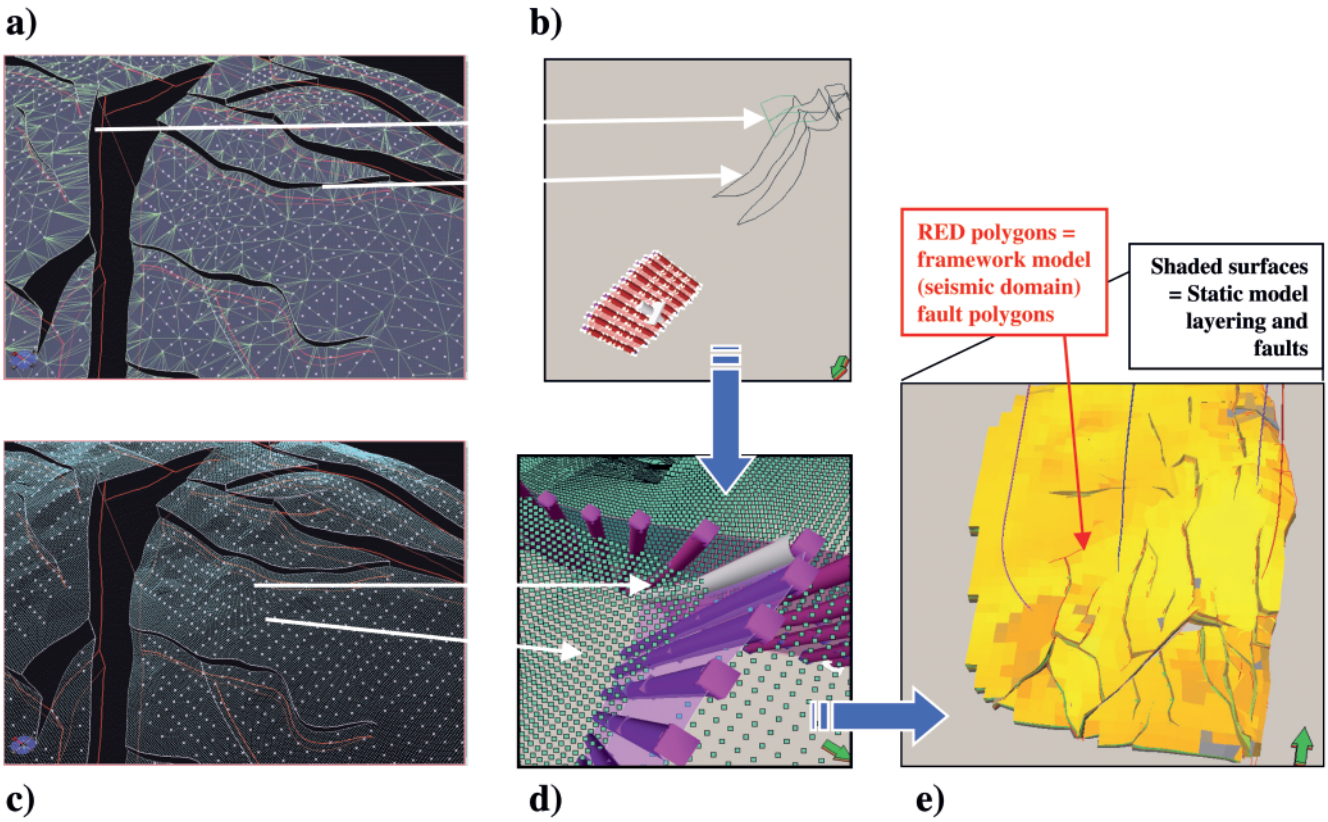

Fig. 12. Structural validity and consistency between seismic interpretation and static modelling. (**a**) Build and validate a structure framework (fault-horizon) model in conjunction with the seismic interpretation, using software specifically designed to model and validate structural geometries. (**b**) Import the framework fault polygons into the static model and re-instate the geocellular fault model from the polygons. (**c**) Up-sample the framework horizon surfaces as x–y–z point data. (**d**) Import these up-sampled point data into the static model where they should fit snugly between all the faults generated from the polygons. Grid the static geocellular horizons from these data. (**e**) Comparison of the modelled horizons and faults with the input data derived from the framework model (actually a close proxy for the seismic interpretation) should show a strong geometrical correspondence. Static model surfaces and faults can also be viewed within the seismic domain to confirm.

SYSTEMATIC MODELLING OF FAULT TRANSMISSIBILITIES

Accurate rendering of fault juxtapositions within Brent Group reservoir models is critical to understanding the brute connectivity of flow units. The permeability of fault zones should also be modelled, using algorithms based on the clay content of fault rocks, as a basis for calculating the transmissibility of faults within simulation models.

Fault clay content and permeability

Given the relationship between clay content and permeability of fault rocks in Brent reservoirs (Fig. 9), it is clear that an understanding of the clay distribution within the faults is critical to modelling flow-retarding effects of the faults in the flow simulator. There are several published and proprietary algorithms available, which calculate the clay content of model-scale fault planes in siliciclastic rocks (see Yielding *et al.* 1997, for discussion). These are based on the entrainment of clay into faults from discrete shale layers and upscaled clay content within the adjacent model layering. Therefore, these algorithms are sensitive to the accuracy of modelled fault displacement and to the petrophysical calculation, upscaling and gridding of V_{shale} (used as a proxy for clay percent); and are effectively reliant upon a geologically feasible upscale of a valid structural-stratigraphic model as described above. The algorithms each focus on the effects of several key physical processes that operate within fault zones (e.g. Figs 7, 8) and are therefore best used in combination to capture the full range of clay entrainment mechanisms active within the faults being modelled. A full discussion of the advantages and disadvantages of each method is outside the scope of this paper, since all have their merits when used within the geological settings for which they were designed (e.g. Fisher & Jolley 2007). Instead, the algorithms used in the context of the work described in this paper are summarized.

The most accessible algorithm is the 'Shale Gouge Ratio' (SGR; Fristad *et al.* 1997; Yielding *et al.* 1997), which focuses on the process of abrasion of relatively soft shale layers and the consequent admixture of collective stratigraphic clay content in the fault plane. This appeals to the redistribution of clay within fault rocks (cf. Fisher & Knipe 1998), the key assumption being that the volume-percent of clay entrained into the collective fault plane at any point along its surface is equivalent to the proportion of shale within the stratigraphy that has slipped past that point (Fig. 14). This may be a fair approximation, since recent comparison of a range of algorithm predictions with geological mapping/logging of surface exposures has shown that SGR gives a reasonable overall match to the average clay content of natural faults (Doughty 2003; van der Zee & Urai 2005).

However, 'shale smear' is another key deformation process that occurs within faults active at relatively shallow burial depths in well-bedded sand–shale sequences (Figs 7 & 8). This process shears the discrete sand and shale layers to form continuous smears within the fault planes. There is often a degree of local complexity in the fault zone around a shale

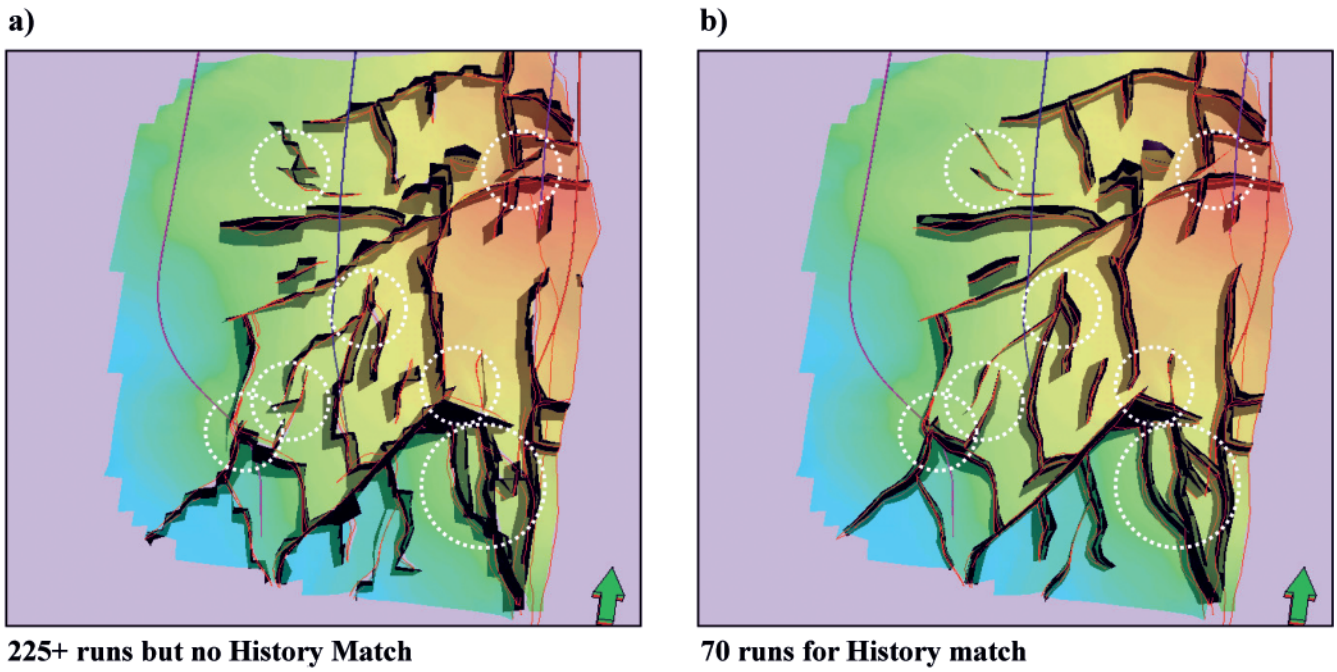

Fig. 13. Static model surface (Top Etive), together with framework model faults derived from the seismic interpretation (red fault polygon lines) that were used to build the static model faults, plus the equivalent fault surfaces from the simulation model (black 'blades') that were derived from them, all loaded into the static model for 3D visualization. This figure illustrates the benefits of preserving structural geometries from seismic interpretation and framework model to static model to simulation model. (**a**) Case 1: The static model was upscaled into the simulator, compromising the integrity of the static horizon-fault model and, therefore, the arrangement of juxtapositions in the model. This is particularly well illustrated in the dotted circles, where simulation model faults either link or open inappropriately across framework fault polygons. No production history match could be achieved in more than 225 runs with this model. This was despite the reservoir engineer amending fault geometries and treating their transmissibility multipliers separately to steer flow around the model and applying a long list of *ad hoc* amendments – many of which exceeded geologically reasonable limits (e.g. 5× permeability multiplier on all layers in the model to get it to flow). (**b**) Case 2: The static model was built to honour the fault geometries at the cell size used in the simulation model (no lateral upscaling). Note that the simulator faults directly overly the original geometrically valid framework fault polygons. Almost none of the previous *ad hoc* amendments were required in the simulator. For example, model layer permeability multipliers were not needed, and only one fault required *ad hoc* treatment. Each simulation run was about 50% faster than the previous model and the model came close to history match in 70 runs, which included testing various sensitivities, before the exercise was terminated.

smear, including overlapping of multiple fault strands across the shale layer. In crude terms, the clay is squeezed like toothpaste from the more pliable shale 'source' layers into the fault zone, where it is stretched out as the fault moves (e.g. Lehner & Pilaar 1997; Aydin & Eyal 2002; van der Zee *et al.* 2003; van der Zee & Urai 2005; Childs *et al.* 2007). Thus, in section view, the shale layers are seen to tongue into the fault and nip-out some distance away from the source bed as the tensile coherency of the material is exceeded by the displacement. Sand beds deformed under shallow burial conditions are also seen to be smeared.

There is a great deal of complexity involved in the ratio of sand versus shale smears, their relative lengths with respect to source-bed thickness, and their lateral continuity (e.g. van der Zee *et al.* 2003; Kristensen 2005). These features are captured for the static and dynamic models by a number of public and proprietary algorithms. For example, the 'Clay Smear Potential' (CSP) algorithm relates the downthrow continuity (length) of a shale smear as a function of the shale source-bed thickness (Fig. 14; Bouvier *et al.* 1989; Fulljames *et al.* 1997; Yielding *et al.* 1997). A related algorithm, the 'Shale Smear Factor' (SSF), calculates smear thickness as a function of fault throw and source layer thickness in order to estimate the continuity of smears caused by abrasion of shales and coals against more resistive sandstones during fault movement under deeper (>2 km burial) conditions (Fig. 14; Lindsay *et al.* 1993; Yielding *et al.* 1997). If a cut-off value is applied as a threshold between 'seal' and 'no-seal', CSP and SSF produce a 'binary' arrangement of totally sealed and 'totally open to flow' bands across the fault planes in a model, based on the ratio of fault throw to thickness distribution of discretely modelled shale source layers. Therefore, these algorithms are extremely sensitive to the validity and accuracy of the modelled layering scheme and fault throw variations.

Once displacement becomes large enough to disengage smears from their source layers, they become entrained wholly or partially within the fault to be randomly parked as sand and clay 'slugs' within the fault plane. However, some outcrop observations do not show a systematic arrangement of clay smears in relation to their source beds, and so a stochastic approach is used to 'place' the smear distributions along the fault planes (Childs *et al.* 2007). In situations such as this, and where the shales are thin within dominantly sand stratigraphy (or *vice versa*), or sand–shale layering is relatively fine (cm–m scale), it can be argued that the smear and slug lengths will be up to orders of magnitude less than fault throw values and are thus accounted for within the SGR algorithm once stratigraphy is upscaled. This implies that SGR can be used under the right circumstances as a catch-all algorithm for estimating fault permeability (e.g. Childs *et al.* 2007). However, in the case of decametre (>10 m scale) thickness sand–shale units deformed by meso-scale to relatively small seismic-scale fault throws, the fault throw to thickness ratio is within 4 or 5, so that sand and shale smears are generally continuous features (cf. Færseth 2006). Under these circumstances, the fault plane is sealed completely across the shale smears and stratigraphic continuity

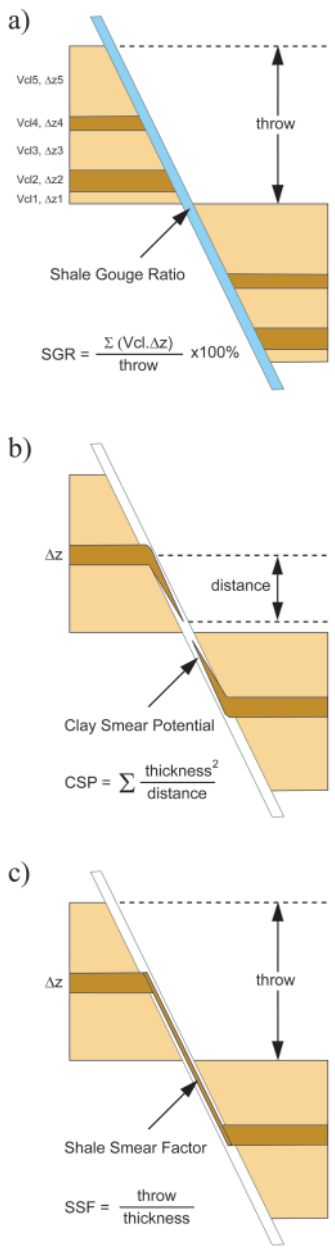

Fig. 14. Fault seal algorithms, commonly applied in low/mid net-to-gross (mixed sand–shale) reservoir stratigraphies: (**a**) Shale Gouge Ratio (SGR, Yielding *et al.* 1997); (**b**) Clay Smear Potential (CSP, Bouvier *et al.* 1989; Fulljames *et al.* 1997); (**c**) Shale Smear Factor (SSF, Lindsay *et al.* 1993).

is maintained – such that the flow integrity of sands and significant shales such as the Mid-Ness-Shale (i.e. stratigraphic compartmentalization), is preserved in the reservoir, despite faulting.

Fault transmissibility

It is possible to calculate the variation of clay values (and related fault permeability distribution) across fault planes in the simulation model from its faulted corner-point structure (e.g. Manzocchi *et al.* 1999). This method uses the dynamic model's geocellular geometry and property grids to calculate unique CSP/SSF, SGR and fault permeability values for each faulted cell face in the model. To do this, the method first compares fault throws that are explicit within the geocellular model construction (from the model corner-point $x/y/z$ and non-neighbour cell connection tables) with the properties of the stratigraphic layering (e.g. net-to-gross, V_{shale}, porosity, permeability). This calculates unique CSP/SSF and SGR values for each explicitly faulted cell face in the model. These values are then used as a proxy for clay percent in order to assign fault permeability values derived from measured data (e.g. Fig. 9). Then the fault rock thickness is also calculated on a cell-by-cell basis as a function of the throw value recorded at each faulted cell face. This simplifies the 3D complexity of the fault rock distribution within the substructure of fault zones by representing the total thickness of fault rock with a single thickness value (cf. Manzocchi *et al.* 1999; Odling *et al.* 2004). The SGR and related fault permeability values are combined with fault rock thickness to calculate unique fault transmissibility multiplier values for each faulted cell connection in the model (Figs 2, 15; as per Manzocchi *et al.* 1999, 2002). Then clay smears can be plotted as/if appropriate on the fault planes to define basic flow/no-flow zones, thus blanking-off certain areas of the fault to flow. This produces a systematic, geologically reasoned and calculated variation of fault transmissibilities within the model, which are then included in the simulation run of that model.

We have applied systematically modelled fault transmissibility multipliers to geometrically valid models (as defined above). To avoid ambiguity in describing the impact of these methods on flow simulations, in this paper we have: (1) included examples from fields with extensive well and production data control (e.g. the Brent Field, with >30 years of production and over 320 wells, and over 8000 well picks in the reservoir model); and (2) concentrated on the early simulation results – at a stage in the history matching process that has few, if any, model edits. In particular, the effects of applying multipliers derived from SGR were examined, since this is a simpler calculation and not as sensitive as CSP or SSF to the choice and upscaling of a modelled V_{shale} layering scheme or to minor fault throw uncertainties. By focusing on SGR in this way, the study has also avoided additional ambiguities arising from the uncertainty associated with stochastic modelling required to place clay smear 'slugs' within fault throw windows (e.g. Childs *et al.* 2007; Manzocchi *et al.* 2007).

Results were compared between models simulated with systematically modelled multipliers derived from 'amalgamation' case fault permeability data and locally derived fault permeability data (e.g. Fig. 9, cf. Fig. 15). In both cases, fault rock thickness (t_f) is assumed to be a linear function of fault throw (D). Following the discussion provided by Manzocchi *et al.* (1999), several t_f scenarios were modelled using the relationships $t_f = D/66$, $D/100$ and $D/170$. It was found that these differences had very little effect on the simulation results compared to the more profound impacts caused by perturbing model geometries and choosing different fault permeability relations. In the amalgamation data case (Fig. 9a), fault permeability (k_f) was given by (Manzocchi *et al.* 1999):

$$\log(k_f) = 0.4 - 4SGR - 0.25\log(D)(1 - SGR)^5. \quad (1)$$

In the case of fault permeability data collected from 'local' drill cores in Brent Group rocks, as discussed above, there is a basic relationship between k_f and clay % of the samples, and also a crude relationship to the depth that the specimens were collected from in the wells (Fig. 9b–d). Thus, in this case, fault permeability in mD, is given by:

$$k_f = a \times SGR^{-b}, \quad (2)$$

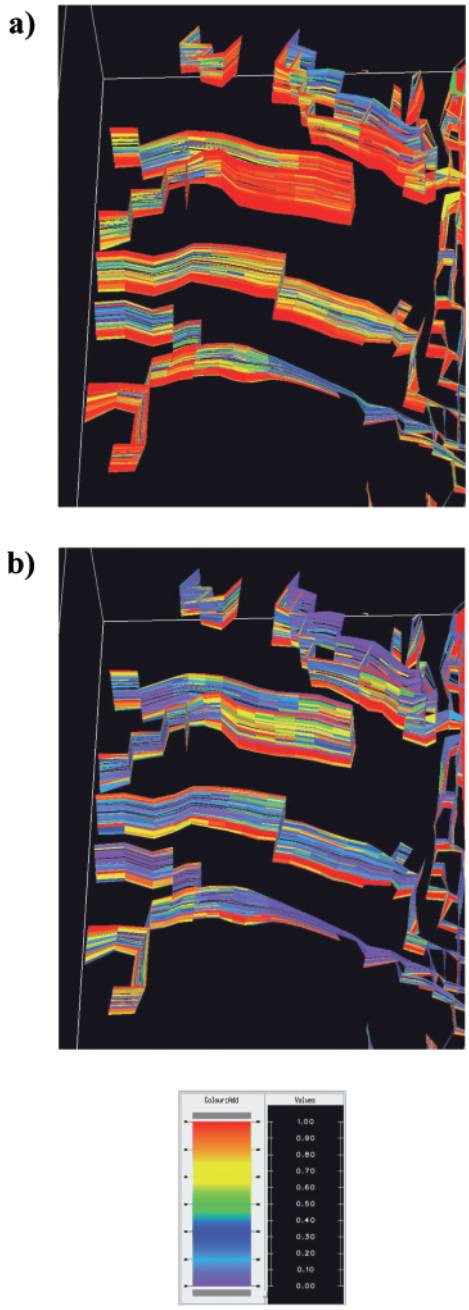

Fig. 15. Perspective 3D views of fault planes in a Brent Field simulation model (layers hidden for clarity). The colours are fault transmissibility multipliers calculated systematically within the simulator, on a cell-by-cell basis to give unique multiplier values for each faulted cell face in the model. (**a**) Multipliers calculated using a basic amalgamated fault permeability data relation described by Manzocchi *et al.* 1999 (cf. Fig. 9a). (**b**) Multipliers calculated based on fault rock data measured from drill core within Brent Group reservoirs (cf. Fig. 9d). Note that, overall, (a) provides more 'open' homogeneous multiplier values and (b) provides more texture in the value distributions – with open high permeability patches in otherwise more flow restrictive fault planes.

where a and b are the position and curvature coefficients of the power-law relations between k_f and clay % for the data (for which SGR calculated from the simulation corner-point model is a proxy). The coefficients a and b have been found to vary as a function of the burial depth-range of the data (Fig. 9d).

Thus, for most of the relations derived from this particular dataset, a ranges between 10^{-5} mD and 10^{-4} mD, and b ranges between 3.5 and 4. From this, it has been possible to use the known burial range of a study reservoir to establish a geologically rationalized base case and a high and low case for fault transmissibility multipliers, derived from the locally acquired fault permeability data, which are quite specific to the geological situation of the reservoir under study. The relations which fit the data are bounded on the low permeability side by the parameter pair $(a, b)=(10^{-5}, 3.5)$ and, on the high side, by $(a, b)=(10^{-4}, 4)$ (Fig. 9d). For example, the relation that would apply as a base case for the whole dataset (2.1–4.3 km sampling depths) would be $k_f = 4\times10^{-5}\times SGR^{-3.47}$. A base case for the Brent and North Cormorant reservoirs, using a sample depth range of 2.5–3.0 km to broadly fit the burial range experienced by these fields, would be $k_f = 10^{-4}\times SGR^{-3.67}$. Compare this to a deeper field, such as Pelican, which might be captured by a base case derived from data in the 3–4 km range to give $k_f = 10^{-5}\times SGR^{-4.07}$ (Fig. 9d). An artefact of these relations is that the fault permeability becomes extremely large to infinite at very low SGR values. Therefore, the fault permeability is capped using the host reservoir sand permeability as a guide.

Simulation results

It is a general observation from production data that fluids and pressures within flow units in the upper Ness and Tarbert sands are often compartmentalized from flow units in the lower Ness and Etive sands. Whilst depletion is often experienced within a flow unit over a wider area than individual small fault blocks, compartments arise during production that are bound within the larger fault blocks in the field (e.g. Fig. 16). This preservation of stratigraphic compartmentalization is explained most logically by clay smear processes on the smaller fault population (as described above). The faults at this scale clearly are not complete barriers to flow, but rather act as flow-retarding 'baffles' within the individual reservoir layers.

Initial simulation runs using a 'traditional' manual application of a fault transmissibility multiplier of 0.01 or 0.02 to all faults in the model will often help provide a starting point for the engineer to gain a certain level of overall pressure match. This is more useful in fields with a fairly homogeneous reservoir stratigraphy, but less successful where the reservoir stratigraphy is more heterogeneous. The results often indicate that the pressures within flow units in the models are too close by comparison with the true 'layered' and larger (km-scale) fault block-bounded pressure compartmentalization seen in the fields. This homogeneous pressure results from faults being too 'open' and thus allowing potential flow paths through the fault systems where they should be sealed. Therefore, fault transmissibility reduction is required to achieve a pressure match between the model and the historical data. However, it is clear that this also induces errors in the 'plumbing' of flow units across the faults, with some faults becoming sealed too much in some areas and left too open to flow in other areas. Moreover – and as pointed out by Manzocchi *et al.* (1999) – a constant transmissibility multiplier applied to a heterogeneous reservoir sequence does not, as generally assumed by the engineer, imply a homogeneous fault. In fact, it implies implicitly that the fault is heterogeneous, but that this heterogeneity has no geological basis and is simply a reflection of the permeabilities of the juxtaposed cells.

The general conclusions that can be drawn from these points are that the flow-retarding effects of faults depend on the particular intra-Brent juxtapositions present; and that the multipliers calculated according to the 'traditional' approach can never come close to honouring natural (yet, in a broad sense,

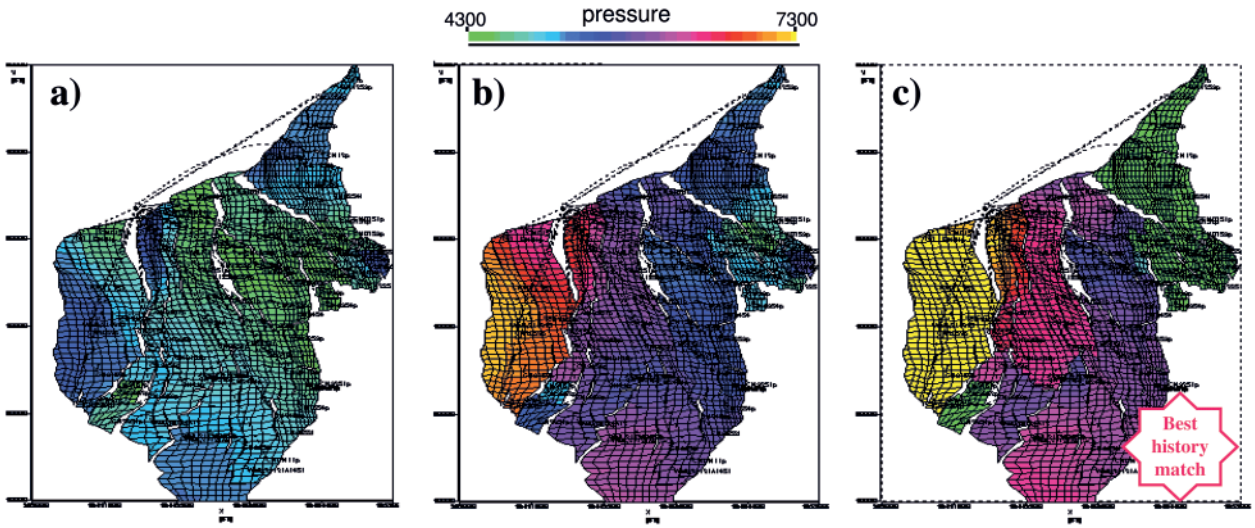

Fig. 16. Pressure history maps from the same time step in production simulation of the North Cormorant Field. (**a**) Simulation based on stratigraphic juxtapositions alone. (**b**) Simulation based on multipliers derived from amalgamated fault permeability data (cf. Figs 9a, 15a). Pressure distribution within this simulation is fairly homogeneous. (**c**) Simulation based on multipliers derived from Brent Group specific fault permeability data (cf. Figs 9d, 15b). Pressure distribution within this simulation contains more extreme pressure values and is compartmentalized more clearly by the faults in the field. This produced the best history match.

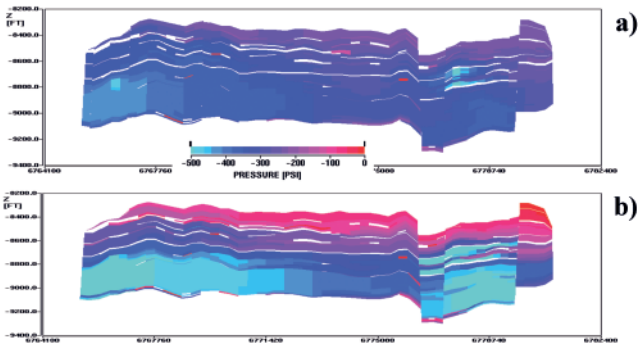

Fig. 17. West–east cross-sections taken from simulation models of the Brent Field. These cross-sections show pressure distribution at the same time step in production simulation. (**a**) 'Traditional' application of global multiplier values result in homogeneous pressure distributions. (**b**) Model run with application of multipliers which were systematically modelled within the simulator, as described in the text. This results in more textured pressure value distributions in the model, which give a significantly better match with actual production data.

predictable) distributions of the sealed portions of faults, or the permeability and thickness of the open but baffling portions. That is best achieved through a 'systematic' approach similar to the one described in this paper (and elsewhere, e.g. Manzocchi *et al.* 1999).

Simulations run on models with application of the systematic fault transmissibility multipliers typically show a more realistic rate distribution of pressure depletion than is achieved by 'traditional' methods (e.g. Fig. 17). The match between the simulated and measured data is enhanced much further where the multipliers are calculated from fault permeability data collected locally from the same or nearby Brent Group reservoirs – where these have experienced similar burial–strain histories (e.g. Fig. 9, cf. Figs 16, 18). Significant differences in simulated pressure depletion emerge between layers, comparable to the measured data (e.g. Fig. 19). The flow pattern steered by the systematic multipliers also improves the fluid production history match. For example, at the Brent Field, where water is used as the key match indicator, data records gave overall water production of 1331 MMBL at the beginning of 2004. If the simulation is run with simple fault treatment (relying on juxtapositions and globally applied single value multipliers), then the modelled water production would have a 143 MMBL shortfall (−10.7% error). This was significantly improved by applying systematically modelled fault transmissibility multipliers (using local fault permeability data), which gave only a 23 MMBL water shortfall (−1.7% error).

Figure 20 shows history match by water production for one of the platforms in the Brent Field. It indicates that whilst there is an improvement in the history match (over simple traditional fault seal treatment) through application of systematically modelled multipliers derived from amalgamation case datasets, there is a significant step-change in improvement of the match where these multipliers are calculated from fault permeability data derived from this and nearby Brent reservoirs. The improvement is especially enhanced where these data come from reservoirs that have experienced similar burial–strain histories. The multipliers produce a clear variability of fluid production across the faults in Brent reservoirs, with more heterogeneous distributions generated in the fault-dominated areas of the fields, and focusing of flow where previously the sweep was more unrealistically uniform.

Following this stage of applying field- and platform-scale adjustments (including the systematic fault transmissibilities described here), the history matches we have illustrated were improved upon further with relatively minor adjustments to the models (Table 1). For example, some well locations and perforation depths are found to be in error, such that too much water is injected into the inappropriate layers in the model. This issue is exacerbated where fracturing during water injection acts to re-connect and equilibrate depletion of local fault/layer compartments in the subsurface but not in the model (see Fig. 18). These issues are addressed by pragmatic adjustment to well locations and perforations, for example, to replicate the locally anomalous pressure/fluid sweep patterns in the model.

DISCUSSION

The mature nature of the fields has provided us with a wealth of structural, stratigraphic and production data, sufficient to test

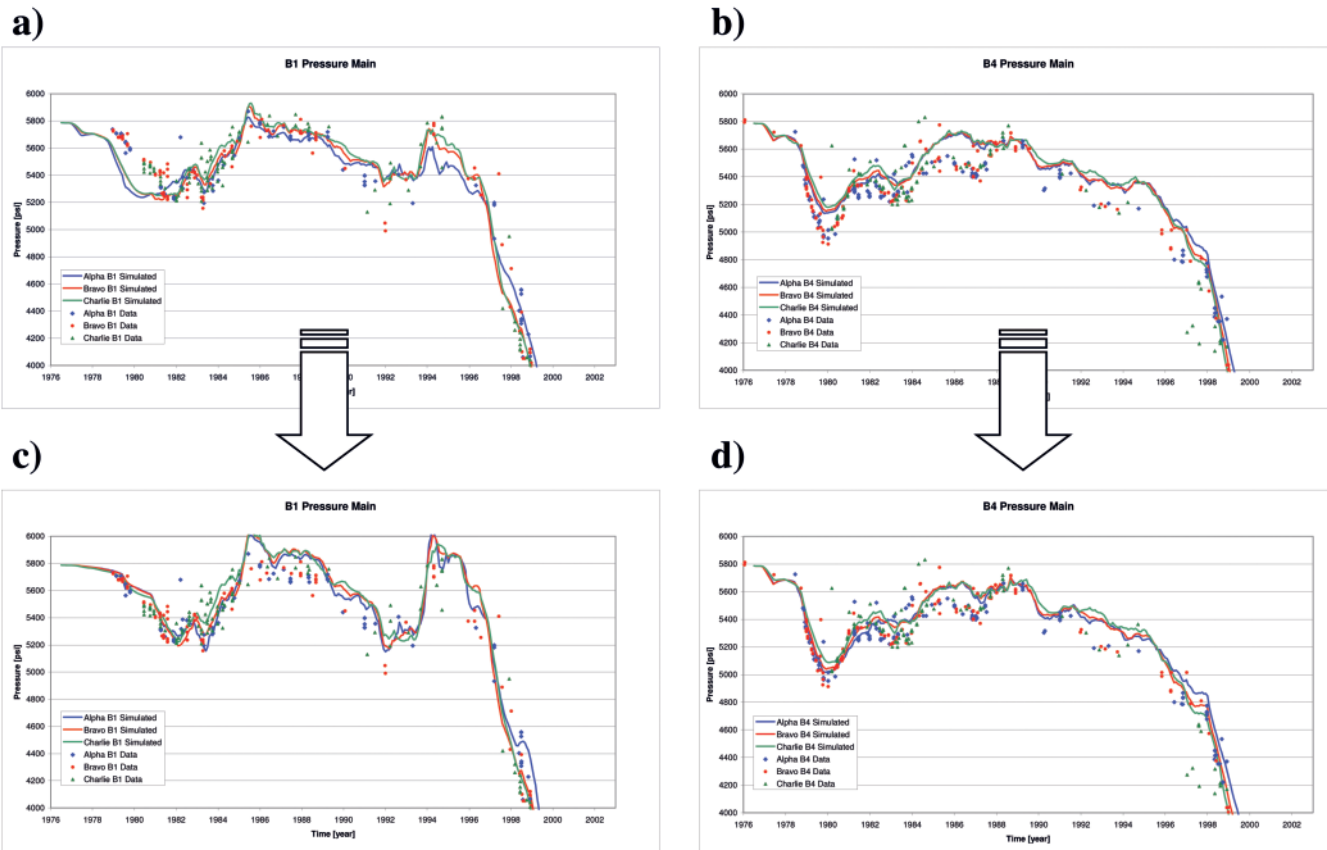

Fig. 18. Simulated pressure history versus actual pressure history data for two key reservoir cycles (flow units) for Alpha, Bravo and Charlie platforms, Brent Field. (**a**, **b**) Imperfect matches achieved through best endeavours using 'traditional' matching methods. (**c**, **d**) Greatly improved fit of the simulation to the data cloud by removing all but the essential *ad hoc* amendments and then re-running the simulation again, including systematically modelled multipliers, based on Brent Group specific fault permeability data. This represents a step-change improvement in the technical quality of the history match and the time taken to achieve it. Some of the local mismatches (e.g. around 1986 and 1992) are related to non-geological factors, such as incorrect well deviation surveys used in the model, or fracturing of the formation during injection causing re-connection of flow units in the field, but not in the model. Most of these features were addressed separately later in the project.

the sensitivity of the dynamic models to a variety of subsurface influences. Stratigraphic architectures and properties and fault juxtaposition architectures are the first line of sensitivity in the simulation, since they impact the fundamental 'plumbing' of the reservoir and also form the basis for fault-seal calculations. Variation in these parameters, therefore, strongly influences the flow baffling-sealing behaviour of the faults.

We have described how geologically reasoned single-phase fault transmissibility multipliers can be calculated from the upscaled corner-point geocellular grid (cf. Manzocchi *et al.* 1999). The positive results described are unambiguous in the main part because effort was put into capturing, validating and preserving the detail of the structural-stratigraphic architecture from the seismic and well data into the static model; and because the subsequent upscaling process was sensitive to the validated fault architectures, thus preserving the arrangement of fault juxtapositions from the seismic interpretation into the static model and through to the simulator (Fig. 21). It follows that aggressive upscaling of a static model erodes the structural coherency of the model geometries and property layering system that the fault seal implementation technique – described here – uses as input data. Thus, although outside the scope of this paper to describe in detail, it is important to note that there is little improvement in history match with this technique when applied to a simulation model that is a poor reflection of the validated structural static model. For integration of fault seal into a simulator to succeed, it is therefore a prior requirement that a geometrically robust structural static model is translated accurately through the upscaling process.

Calculation of multipliers from the upscaled corner-point geocellular grid results in a unique multiplier per faulted cell connection in the model. As such this provides a mimic for the 'texture' of variation in cross-fault flow baffling effects that are likely to characterize the surface of geological faults – as suggested by the complex distribution of sub-structures and fault rock products within natural fault zones. The overall severity of the baffling and the degree of homogenization or granularity in the spatial variation between neighbouring multiplier values in this 'texture' is a function of the SGR–fault permeability (k_f) data relation applied to the SGR values on the faults.

Of the various scenarios tested, those that compare SGR with published amalgamated fault permeability data are capable of improving the production history match. However, a step-change improvement in the match is achieved by SGR comparison with fault permeability data derived from sources local to the reservoir/field under study (in this case, data collected from faults in nearby Brent Group reservoirs). The improvement is particularly enhanced when the data included are derived from fault rocks formed under similar burial depths and which experienced similar burial (stress–temperature) histories to the study reservoir (cf. Figs 9, 20).

The intuitive explanation for this is that the Brent fault rock data came from reservoir rocks and deformation features that

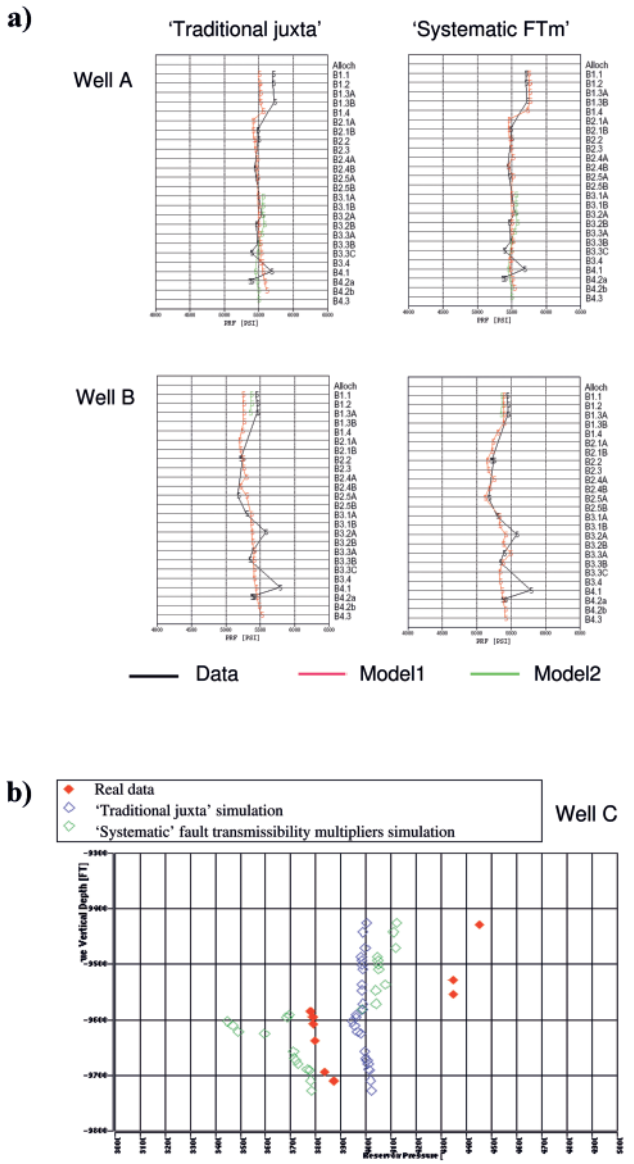

Fig. 19. Comparison of pressures simulated by the 'traditional' history match approach and systematic approach using Brent Group specific fault rock data, against actual pressure data measured by RFT. (**a**) Two wells from the Brent Field. Note that the shape of the simulated pressure profile in the wells has a better fit with the actual pressure data, where systematically modelled fault transmissibilities have been incorporated into the model. (**b**) Well from the North Cormorant Field. Again, note the homogeneous model pressure profile produced by 'traditional' simulation methods, and the better fit between the shape of the modelled pressure profile and the actual pressure data where systematically modelled fault transmissibilities have been used in the simulation.

have similar host mineralogies and physical attributes, and which had experienced essentially the same burial, diagenetic and strain histories and produced the same suite of deformation mechanisms to the faults in the reservoir being modelled. Following this logic, one can expect that the SGR–k_f relation should vary between basins and host stratigraphies in response to variation in this suite of factors. The 'global' amalgamated datasets thus bring together a myriad of different mineralogies, geological conditions, strain–burial histories and physical-chemical mechanisms and different data collection and processing methods (e.g. Fig. 20; cf. Manzocchi *et al.* 1999, fig. 2). The resulting SGR–k_f relation indicates what ideal 'hybrid' faults would be like if lots of different basin types, stratigraphies and strain–burial histories were combined together. Taken in isolation, the motif of each dataset in an amalgamated data cloud is unique to the local situation, with only some being similar to the 'amalgamation case'. Therefore, as discussed by Manzocchi *et al.* (1999), while the amalgamation case might be a pragmatic approach with accepted uncertainties in relatively unknown reservoirs or otherwise sparse data situations, it is clearly preferable to use locally derived data, if available.

Several recent studies have suggested that it may sometimes be necessary to take into account the multi-phase flow properties of fault rocks during production simulation modelling (e.g. Manzocchi *et al.* 1998, 2002; Manzocchi 1999; Fisher & Knipe 2001; Rivenæs & Dart 2002; Al-Busafi *et al.* 2005). History matches were obtained rapidly within the present study using transmissibility multipliers based on single-phase measures of fault rock permeability, without taking into account either their capillary pressure or relative permeability characteristics. The results of this study should not, however, be taken as providing justification for discounting the importance of multi-phase flow properties of faults in all production simulation models. Simple models, in which injector–producer well pairs are situated on either side of faults, with low permeabilities and high capillary entry pressures, also indicate that taking into account the multi-phase flow properties of faults is less important than fault rock thickness and absolute permeability (Al-Busafi *et al.* 2005). However, in other situations, such as reservoirs with little/no shale content and/or where reservoirs are produced by aquifer support or gas expansion, taking into account multi-phase flow is far more important (e.g. Zijlstra *et al.* 2007). The difference between these situations is that where injector–producer pairs are present, flow rates are sufficiently high that viscous forces dominate flow. Where lower flow rates are present, capillary forces will dominate and, in such situations, it is far more important to take into account the multi-phase flow behaviour of the faults (Manzocchi *et al.* 1998, 2002).

CONCLUSIONS

From a theoretical standpoint and by comparison with historical production data, results indicate that systematic modelling of single-phase fault transmissibility multipliers from the cellular model enables rapid application of fault seal to simulation models. Compared with 'traditional' methods, this allows superior production history match results to be achieved with far less manual intervention, and at a fraction of the normal workflow speed. Given the improvement in technical product and speed to achieve history match, this leads to improved confidence and quality of field development and management decisions based on running the models in predictive mode.

The Brent Group fields contain a complex arrangement of fault juxtapositions of the well-layered sand–shale reservoir stratigraphy. These juxtapositions are a first-order sensitivity on compartmentalization of pressures and fluid flow within production simulation models of the reservoirs. The detail of fault-horizon geometries should, therefore, be captured and geologically validated from the seismic interpretation through to the static geocellular model by framework model building in conjunction with the interpretation. This geometrical information should be preserved through the upscaling process into the simulation model because it captures the 'plumbing' of the faulted layering system in the model. It is also critical input data used for calculating fault zone clay content and subsequent fault transmissibility multipliers from the upscaled grid for use in the production simulation. Application of these multipliers to

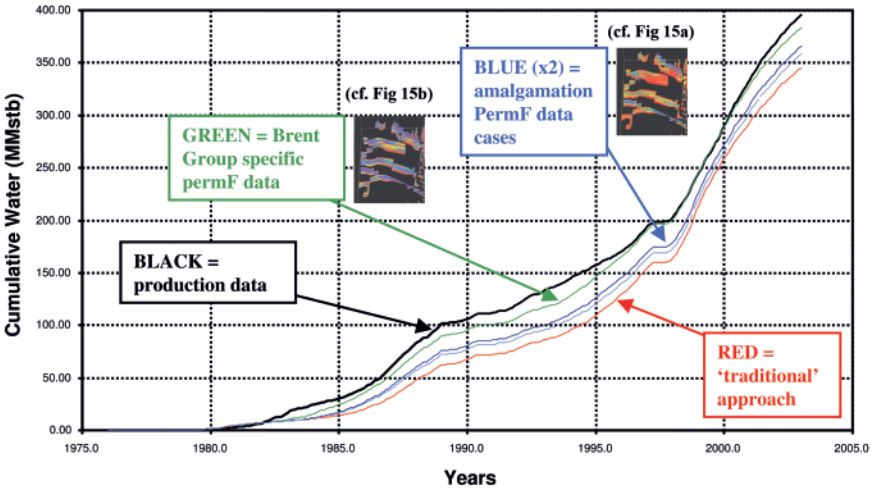

Fig. 20. Production history match measured by water production for one of the platforms on the Brent Field. Note that incorporating systematically modelled fault transmissibilities in the simulation improves the match to actual production data (compared to the result from the 'traditional' approach). Of the systematic approaches, use of amalgamated fault rock permeability data (cf. Figs 9a, 15a) improves the match, whereas use of fault rock permeability data measured directly from Brent Group reservoir cores (cf. Figs 9d, 15b) results in a step-change improvement in the match.

Table 1. *Basic simulation model adjustments applied at three broad scales and stages*

Field-scale (early)	Systematic fault transmissibility multipliers
	Aquifer strength and critical saturation assessments
	Relative permeability curves for well inflow
Platform/layer-scale (early/mid)	Layer permeability–transmissibility multiplications
Well-scale (late)	Adjustments on well location, well perforation depths, well bore k_h
	Modifications on grid block (non-neighbour or neighbour) connections and permeability
	Improvements of well voidage match and well predictions

geometrically weak models tends to produce ambiguous or otherwise potentially misleading simulation results.

Several case examples of mature Brent Group fields were used to illustrate: (a) the effectiveness of systematic modelling of fault transmissibility multipliers in capturing the essential fluid flow properties of faults and faulted reservoir connectivity for simulation models; and (b) that this is capable of generating a step-change improvement in production history match without requiring for further significant iterative *ad hoc* edits to model parameters. Specifically, single-phase fault transmissibility multipliers were incorporated that had been calculated systematically from fault throw/thickness ratios and the SGR derived from the upscaled geocellular grid, by comparing the SGR with data that correlate fault permeability with clay content.

In summary, a step-change improvement in the speed and quality of a history match is achieved where:

- geometrical coherence is ensured and preserved between the seismic interpretation, static geocellular model and the production simulation model by model building and validation in conjunction with seismic interpretation, and by sensitive upscaling to preserve these geometries for input to the simulator;
- fluid flow properties of the faults are accounted for in the simulator by systematic modelling of fault transmissibility multipliers from the upscaled geocellular geometry/property grids in the model, to produce unique multiplier values for each faulted cell face;
- multipliers calculated on 'amalgamation' datasets, based on global correlations between fault permeability and clay content improved the history match. However, the history match was far better when these multipliers were calculated with reference to fault rock permeability–clay content data,

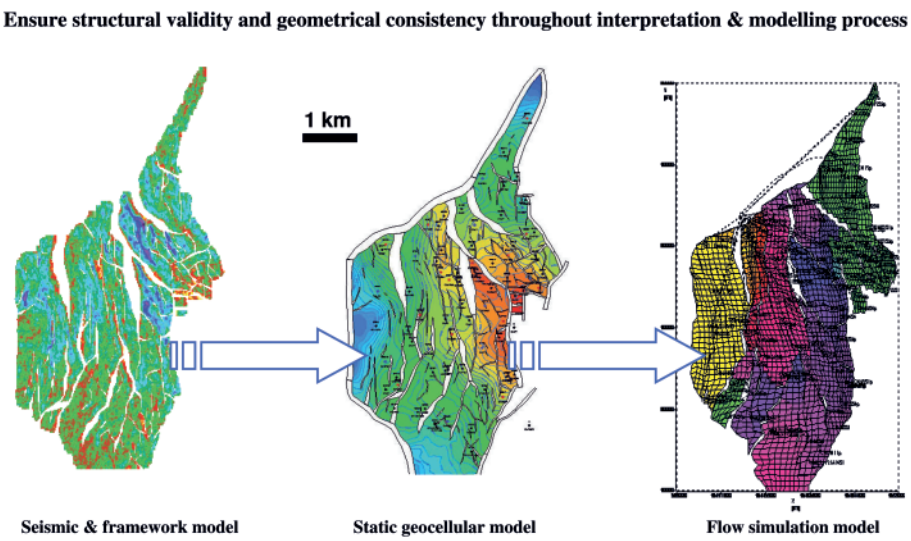

Fig. 21. Achieving geometrical validity in seismic interpretation of horizons and faults and preserving this geometry through the static geocellular model and into the simulator. This is the key structural sensitivity in achieving a production history match since it directly impacts the 'plumbing' of flow unit juxtapositions and the fault seal calculation in the simulation model.

measured from faults present in drill cores within the study reservoir, and/or from similar reservoirs within the same stratigraphy in nearby fields in the region. The results are particularly enhanced where these data are measured from rocks that have experienced a similar burial–strain history to the study reservoir.

The results summarized in this paper are a by-product of our structural work on 'live' asset projects during 2001–2004. The authors thank predecessors and office co-habitants who have worked with them on these fields, for their part in supporting this study, (in particular Simon Price, Hans de Keijzer, Tim Stevens, and Adrian Crawford, Rob Staples, Eric Leoutre, John Horsburgh, Nirmal Jethwa, Andy Lind, Peter Watson and Clair Woods). The Shell authors also take this opportunity to highlight the benefit of collaboration between ourselves in the operating assets and our academic research colleagues: Quentin Fisher who measured and provided the raw fault rock property data; Tom Manzocchi and Andy Heath who helped with teething problems applying their TransGen software to our in-house simulation package MoReS. Comments from reviewers Graham Yielding, Signe Ottesen and Tony Buller helped improve the manuscript.

REFERENCES

Al-Busafi, B., Fisher, Q.J. & Harris, S.D. 2005. The importance of incorporating the multiphase flow properties of fault rocks into production simulation models. *Marine and Petroleum Geology,* **22**, 365–374.

Aydin, A. & Eyal, Y. 2002. Anatomy of a normal fault with shale smear: implications for fault seal. *American Association of Petroleum Geologists Bulletin,* **86**, 1367–1381.

Beach, A., Welbon, A.I., Brockbank, P.J. & McCallum, J.E. 1999. Reservoir damage around faults: outcrop examples from the Suez rift. *Petroleum Geoscience,* **5**, 109–116.

Bellahsen, N. & Daniela, J.M. 2005. Fault reactivation control on normal fault growth: an experimental study. *Journal of Structural Geology,* **27**, 769–780.

Berg, S.S. & Skar, T. 2005. Controls on damage zone asymmetry of a normal fault zone: outcrop analyses of a segment of the Moab fault, SE Utah. *Journal of Structural Geology,* **27**, 1803–1822.

Berger, M. & Roberts, A.M. 1999. The Zeta structure: a footwall degredation complex formed by gravity sliding on the western margin of the Tampen Spur, northern North Sea. *In:* Fleet, A.J. & Boldy, S.A.R. (eds) *Petroleum Geology of Northwest Europe: Proceedings of the 5th Conference.* Geological Society, London, 106–116.

Bouvier, J.D., Kaars-Sijpesteijn, C.H., Kleusner, D.F., Onyejekwe, C.C. & van der Pal, R.C. 1989. Three-dimensional seismic interpretation, and fault sealing investigations, Nun River field, Nigeria. *American Association of Petroleum Geologists Bulletin,* **73**, 1397–1414.

Caine, J.S., Evans, J.P. & Forster, C.G. 1996. Fault zone architecture and permeability structure. *Geology,* **24**, 1025–1028.

Childs, C., Walsh, J.J. & Watterson, J. 1997. Complexity in fault zone structure and implications for fault seal prediction. *In:* Møller-Pederson, P. & Koestler, A.G. (eds) *Hydrocarbon seals: importance for exploration and production.* Norwegian Petroleum Society (NPF) Special Publication, **7**, 61–72.

Childs, C., Manzocchi, T., Nell, P.A.R., Walsh, J.J., Strand, J.A., Heath, A.E. & Lygren, T.H. 2002. Geological implications of a large pressure difference across a small fault in the Viking Graben. *In:* Koestler, A.G. & Hunsdale, R. (eds) *Hydrocarbon seal quantification.* Norwegian Petroleum Society (NPF) Special Publication, **11**, 127–139.

Childs, C., Walsh, J.J., Manzocchi, T. *et al.* 2007. Definition of a fault permeability predictor from outcrop studies of a faulted turbidite sequence, Taranaki, New Zealand. *In:* Jolley, S.J., Barr, D., Walsh, J.J. & Knipe, R.J. (eds) *Structurally Complex Reservoirs.* Geological Society, London, Special Publications, **292**, 235–258.

Corrigan, A.F. 1993. Estimation of recoverable reserves: the geologist's job. *In:* Parker, J.R. (ed.) *Petroleum Geology of Northwest Europe: Proceedings of the 4th Conference.* Geological Society, London, 1473–1481.

Dake, L.P. 2001. *Practice of reservoir engineering.* Elsevier, New York.

Davatzes, N.C. & Aydin, A. 2005. Distribution and nature of fault architecture in a layered sandstone and shale sequence: an example from the Moab fault, Utah. *In:* Sorkhabi, R. & Tsuji, Y. (eds) *Faults, fluid flow and petroleum traps.* American Association of Petroleum Geologists, Memoir, **85**, 153–180.

Deegan, C.E. & Scull, B.J. 1977. *A proposed standard lithostratigraphic nomenclature for the Central and Northern North Sea.* Report of the Institute of Geological Sciences 77/25 and Bulletin of the Norwegain Petroleum Directorate, No. 1.

Doughty, P.T. 2003. Clay smear seals and fault sealing potential of an exhumed growth fault, Rio Grande rift, New Mexico. *American Association of Petroleum Geologists Bulletin,* **87**, 427–444.

Eichhubl, P., D'Onfro, P.S., Aydin, A., Waters, J. & McCarty, D.K. 2005. Structure, petrophysics, and diagenesis of shale entrained along a normal fault at Black Diamond Mines, California – implications for fault seal. *American Association of Petroleum Geologists Bulletin,* **89**, 1113–1137.

Fisher, Q.J. & Jolley, S.J. 2007. Treatment of faults in production simulation models. *In:* Jolley, S.J., Barr, D., Walsh, J.J. & Knipe, R.J. (eds) *Structurally Complex Reservoirs.* Geological Society, London, Special Publications, **292**, 219–234.

Fisher, Q.J. & Knipe, R.J. 1998. Fault sealing processes in siliciclastic sediments. *In:* Jones, G., Fisher, Q.J. & Knipe, R.J. (eds) *Faulting, Fault Sealing and Fluid Flow in Hydrocarbon Reservoirs.* Geological Society, London, Special Publications, **147**, 117–134.

Fisher, Q.J. & Knipe, R.J. 2001. The permeability of faults within siliciclastic petroleum reservoirs of the North Sea and Norwegian Continental Shelf. *Marine and Petroleum Geology,* **18**, 1063–1081.

Fisher, Q.J., Knipe, R.J. & Worden, R.H. 2000. Microstructures of deformed and non-deformed sandstones from the North Sea: implications for the origins of quartz cement in sandstones. *In:* Worden, R.H. & Morad, S. (eds) *Quartz cementation in sandstones.* Special Publication of the International Association of Sedimentology, **29**, 129–146.

Fisher, Q.J., Harris, S.D., McAllister, E., Knipe, R.J. & Bolton, A.J. 2001. Hydrocarbon flow across faults by capillary leakage revisited. *Marine and Petroleum Geology,* **18**, 251–257.

Foxford, K.A., Walsh, J.J., Watterson, J., Garden, I.R., Guscott, S.C. & Burley, S.D. 1998. Structure and content of the Moab fault Zone, Utah, USA, and its implications for fault seal prediction. *In:* Jones, G., Fisher, Q.J. & Knipe, R.J. (eds) *Faulting, Fault Sealing and Fluid Flow in Hydrocarbon Reservoirs.* Geological Society, London, Special Publications, **147**, 87–103.

Fristad, T., Groth, A., Yielding, G. & Freeman, B. 1997. Quantitative fault seal prediction – a case study from Oseberg Syd. *In:* Moller-Pedersen, P. & Koestler, A.G. (eds) *Hydrocarbon seals: importance for exploration and production.* Norwegian Petroleum Society (NPF) Special Publication, **7**, 107–124.

Fulljames, J.R., Zijerveld, L.J.J. & Franssen, R.C.M.W. 1997. Fault seal process: systematic analysis of fault seals over geological and production time scales. *In:* Moller-Pedersen, P. & Koestler, A.G. (eds) *Hydrocarbon seals: importance for exploration and production.* Norwegian Petroleum Society (NPF) Special Publication, **7**, 51–60.

Færseth, R.B. 1996. Interaction of Permo-Triassic and Jurassic extensional fault-blocks during the development of the northern North Sea. *Journal of the Geological Society, London,* **153**, 931–944.

Færseth, R.B. 2006. Shale smear along large faults: Continuity of smear and the fault seal capacity. *Journal of the Geological Society, London,* **163**, 741–751.

Hampson, G.J., Sixsmith, P.J. & Johnson, H.D. 2004. A sedimentological approach to refining reservoir architecture in a mature hydrocarbon province: the Brent Province, UK North Sea. *Marine and Petroleum Geology,* **21**, 457–484.

Hesthammer, J. & Fossen, H. 1999. Evolution and geometries of gravitational collapse structures with examples from the Statfjord Field, northern North Sea. *Marine and Petroleum Geology,* **16**, 259–281.

Hesthammer, J., Bjørkum, P.A. & Watts, L. 2002. The effect of temperature on sealing capacity of faults in sandstone reservoirs: examples from the Gullfaks and Gullfaks Sør fields, North Sea. *American Association of Petroleum Geologists Bulletin,* **86**, 1733–1751.

Jolley, S.J., Stuart, G.W., Freeman, S.R. *et al.* 2007. Progressive evolution of a late-orogenic thrust system, from duplex development to extensional reactivation and disruption: Witwatersrand Basin, South Africa. *In:* Ries, A.C., Butler, R.W.H. & Graham, R.H. (eds) *Deformation of the Continental Crust.* Geological Society, London, Special Publications, **272**, 543–569.

Khalil, S.M. & McClay, K.R. 2001. Tectonic evolution of the northwestern Red Sea–Gulf of Suez rift system. *In:* Wilson, R.C.L., Whitmarsh, R.B., Taylor, B. & Froitzheim, N. (eds) *Non-volcanic Rifting of Continental Margins: a Comparison of Evidence From Land and Sea.* Geological Society, London, Special Publications, **187**, 453–473.

Kristensen, M.B. 2005. *Soft sediment faulting: investigation of the 3D geometry and fault zone properties.* PhD thesis. University of Aarhus, Denmark.

Lehner, F.K. & Pilaar, W.F. 1997. The emplacement of clay smears in synsedimentary normal faults: inferences from field observations near Frechen, Germany. *In:* Moller-Pedersen, P. & Koestler, A.G. (eds) *Hydrocarbon seals: importance for exploration and production.* Norwegian Petroleum Society (NPF) Special Publication, **7**, 39–50.

Lia, O., Omre, H., Tjelmeland, H., Holden, L. & Egeland, T. 1997. Uncertainties in reservoir production forecasts. *American Association of Petroleum Geologists Bulletin,* **81**, 775–802.

Lindsay, N.G., Murphy, F.C., Walsh, J.J. & Watterson, J. 1993. Outcrop studies of shale smears on fault surfaces. *In:* Flint, S.T. & Bryant, A.D. (eds) *The geological modelling of hydrocarbon reservoirs and outcrop.* Special

Publication of the International Association of Sedimentology, **15**, 113–123.

Lygren, M., Fagervik, K., Valen, T.S. *et al.* 2003. A method for performing history matching of reservoir flow models using 4D seismic data. *Petroleum Geoscience,* **9**, 85–90.

Manzocchi, T. 1999. Towards an Improved Fault Representation in Two-phase Reservoir Simulation. *Extended abstracts 61st EAGE Conference and Technical Exhibition, Helsinki,* **1**, C-05.

Manzocchi, T., Ringrose, P.S. & Underhill, J.R. 1998. Flow through fault systems in high porosity sandstones. *In:* Coward, M.P., Johnson, H. & Daltaban, T. (eds) *Structural Geology in Reservoir Characterization.* Geological Society, London, Special Publications, **127**, 65–82.

Manzocchi, T., Walsh, J.J., Nell, P. & Yielding, G. 1999. Fault transmissibility multipliers for flow simulation models. *Petroleum Geoscience,* **5**, 53–63.

Manzocchi, T., Heath, A.E., Walsh, J.J. & Childs, C. 2002. The representation of two phase fault-rock properties in flow simulation models. *Petroleum Geoscience,* **8**, 119–132.

Manzocchi, T., Walsh, J.J., Tomasso, M., Strand, J., Childs, C. & Haughton, P.D.W. 2007. Static and dynamic connectivity in bed-scale models of faulted and unfaulted turbidites. *In:* Jolley, S.J., Barr, D., Walsh, J.J. & Knipe, R.J. (eds) *Structurally Complex Reservoirs.* Geological Society, London, Special Publications, **292**, 309–336.

McLeod, A.E., Dawers, N.H. & Underhill, J.R. 2000. The propagation and linkage of normal faults: insights from the Strathspey–Brent–Statfjord fault array, northern North Sea. *Basin Research,* **12**, 263–284.

McLeod, A.E., Underhill, J.R., Davies, S.J. & Dawers, N.H. 2002. The influence of fault array evolution on synrift sedimentation patterns: Controls on deposition in the Strathspey–Brent–Statfjord half graben, northern North Sea. *American Association of Petroleum Geologists Bulletin,* **86**, 1061–1093.

Morley, C.K., Haranya, C., Phoosongsee, S., Kornsawan, A. & Wonganan, N. 2004. Activation of rift oblique and rift parallel pre-existing fabrics during extension and their effect on deformation style: examples from the rifts of Thailand. *Journal of Structural Geology,* **26**, 1803–1829.

Needham, D.T., Yielding, G. & Freeman, B. 1996. Analysis of fault geometry and displacement patterns. *In:* Buchanan, P.G. & Nieuwland, D.A. (eds) *Modern Developments in Structural Interpretation, Validation and Modelling.* Geological Society, London, Special Publications, **99**, 189–199.

Odling, N.E., Harris, S.D. & Knipe, R.J. 2004. Permeability scaling properties of fault damage zones in siliciclastic rocks. *Journal of Structural Geology,* **26**, 1727–1747.

Peacock, D.C.P. & Shepherd, J. 1997. Reactivated faults and transfer zones in the Southern Coalfield, Sydney Basin, Australia. *Australian Journal of Earth Sciences,* **44**, 265–273.

Rivenæs, J.C. & Dart, C. 2002. Reservoir compartmentalisation by water-saturated faults – Is evaluation possible with today's tools. *In:* Koestler, A.G. & Hunsdale, R. (eds) *Hydrocarbon seal quantification.* Norwegian Petroleum Society (NPF) Special Publication, **11**, 173–186.

Roberts, A.M., Yielding, G., Kusznir, N.J., Walker, I.M. & Dorn-Lopez, D. 1995. Quantitative analysis of Triassic extension in the northern Viking Graben. *Journal of the Geological Society, London,* **152**, 15–26.

Rutten, K.W. & Verschuren, M.A.J. 2003. Building and unfaulting fault-horizon networks. *In:* Nieuwland, D.A. (ed.) *New Insights into Structural Interpretation and Modelling.* Geological Society, London, Special Publications, **212**, 39–57.

Rykkelid, E. & Fossen, A. 2002. Layer rotation around vertical fault overlap zones: observations from seismic data, field examples, and physical experiments. *Marine and Petroleum Geology,* **19**, 181–192.

Shipton, Z.K., Evans, J.P. & Thompson, L.B. 2005. The geometry and thickness of deformation-band fault core and its influence on sealing characteristics of deformation-band fault zones. *In:* Sorkhabi, R. & Tsuji, Y. (eds) *Faults, fluid flow and petroleum traps.* American Association of Petroleum Geologists, Memoir, **85**, 181–195.

Sperrevik, S., Gillespie, P.A., Fisher, Q.J., Halvorsen, T. & Knipe, R.J. 2002. Empirical estimation of fault rock properties. *In:* Koestler, A.G. & Hunsdale, R. (eds) *Hydrocarbon seal quantification.* Norwegian Petroleum Society (NPF) Special Publication, **11**, 109–125.

Staples, R., Hague, P., Cooke, G. *et al.* 2002. Integrating 4D seismic to optimize production. *Paper,* SPE78346.

Staples, R., Stevens, T., Leoutre, E., Jolley, S.J. & Marshall, J.D. 2005. 4D seismic history matching: the reality. Paper D009, 67th EAGE Conference, Madrid.

Sverdrup, E. & Bjørlykke, K. 1992. Small faults in sandstones from Spitsbergen and Haltenbanken. A study of diagenetic and deformational structures and their relation to fluid flow. *In:* Larsen, R.M., Brekke, H., Larsen, B.T. & Talleraas, E. (eds) *Structural and tectonic modelling and its application to petroleum geology.* Norwegian Petroleum Society (NPF) Special Publication, **1**, 507–517.

Taylor, S.R., Almond, J., Arnott, S., Kemshell, D. & Taylor, D. 2003. The Brent FieldBlock 211/29, UK North Sea. *In:* Gluyas, J.G. & Hichens, H.M. (eds) *United Kingdom Oil and Gas Fields, Commemorative Millennium Volume.* Geological Society, London, Memoir, **20**, 233–250.

Thomson, K. & Underhill, J.R. 1993. Controls on the development and evolution of structural styles in the Inner Moray Firth, UK North Sea. *In:* Parker, J.R. (ed.) *Petroleum Geology of Northwest Europe, Proceedings of the 4th Conference.* Geological Society, London, 1167–1178.

Townsend, C., Firth, I.R., Westerman, R., Kirkevollen, L., Harde, M. & Torill, A. 1998. Small seismic-scale fault identification and mapping. *In:* Jones, G., Fisher, Q.J. & Knipe, R.J. (eds) *Faulting, Fault Sealing and Fluid Flow in Hydrocarbon Reservoirs.* Geological Society, London, Special Publications, **147**, 1–25.

Underhill, J.R., Sawyer, M.J., Hodgson, P., Shallcross, M.D. & Gawthorpe, R.L. 1997. Implications of Fault Scarp Degradation for Brent Group Prospectivity, Ninian Field, Northern North Sea. *American Association of Petroleum Geologists Bulletin,* **81**, 999–1022.

van der Zee, W. & Urai, J.L. 2005. Processes of normal fault evolution in a siliciclastic sequence: a case study from Miri, Sarawak, Malaysia. *Journal of Structural Geology,* **27**, 2281–2300.

van der Zee, W., Urai, J.L. & Richard, P.D. 2003. Lateral clay injection into normal faults. *GeoArabia,* **8**, 501–522.

Waggoner, J.R., Cominelli, A., Seymour, R.H. & Stradiotti, A. 2003. Improved reservoir modelling with time-lapse seismic data in a Gulf of Mexico gas condensate reservoir. *Petroleum Geoscience,* **9**, 61–72.

Welbon, A.I.F., Brockbank, P.J., Brunsden, D. & Olsen, T.S. 2007. Characterising and producing from reservoirs in landslides: challenges and opportunities. *In:* Jolley, S.J., Barr, D., Walsh, J.J. & Knipe, R.J. (eds) *Structurally Complex Reservoirs.* Geological Society, London, Special Publications, **292**, 49–74.

Yielding, G., Badley, M.E. & Roberts, A.M. 1992. The structural evolution of the Brent Province. *In:* Morton, A.C., Haszeldine, R.S., Giles, M.R. & Brown, S. (eds) *Geology of the Brent Group.* Geological Society, London, Special Publications, **61**, 27–43.

Yielding, G., Freeman, B. & Needham, D.T. 1997. Quantitative fault seal prediction. *American Association of Petroleum Geologists Bulletin,* **81**, 897–917.

Younes, A.I. & McClay, K.R. 2002. Development of accommodation zones in the Gulf of Suez–Red Sea rift, Egypt. *American Association of Petroleum Geologists Bulletin,* **86**, 1003–1026.

Ziegler, P.A. 1990. Tectonic and palaeogeographic development of the North Sea rift system. *In:* Blundell, D.J. & Gibbs, A.D. (eds) *Tectonic Evolution of the North Sea Rifts.* Oxford Science Publications, Oxford, 1–36.

Zijlstra, E.B., Reemst, P.H.M. & Fisher, Q.J. 2007. Incorporation of fault properties into production simulation models of Permian reservoirs from the southern North Sea. *In:* Jolley, S.J., Barr, D., Walsh, J.J. & Knipe, R.J. (eds) *Structurally Complex Reservoirs.* Geological Society, London, Special Publications, **292**, 295–308.

Received 10 November 2006; revised typescript accepted 28 June 2007.